



<b>Title</b>	Search for correlations between the optical and radio polarization of active galactic nuclei - I. VLBA polarization data at 15+22+43GHz
<b>Author(s)</b>	Algaba, Juan Carlos; Gabuzda, Denise; Smith, P. S.
<b>Publication date</b>	2011
<b>Original citation</b>	Algaba, J. C., Gabuzda, D. C. and Smith, P. S. (2011) 'Search for correlations between the optical and radio polarization of active galactic nuclei – I. VLBA polarization data at 15 + 22 + 43 GHz', Monthly Notices of the Royal Astronomical Society, 411(1), pp. 85-101. doi: 10.1111/j.1365-2966.2010.17654.x
<b>Type of publication</b>	Article (peer-reviewed)
<b>Link to publisher's version</b>	<a href="https://academic.oup.com/mnras/article-lookup/doi/10.1111/j.1365-2966.2010.17654.x">https://academic.oup.com/mnras/article-lookup/doi/10.1111/j.1365-2966.2010.17654.x</a> <a href="http://dx.doi.org/10.1111/j.1365-2966.2010.17654.x">http://dx.doi.org/10.1111/j.1365-2966.2010.17654.x</a> Access to the full text of the published version may require a subscription.
<b>Rights</b>	© 2010, the Authors. Journal compilation © 2010, RAS
<b>Item downloaded from</b>	<a href="http://hdl.handle.net/10468/4965">http://hdl.handle.net/10468/4965</a>

Downloaded on 2018-08-23T19:08:26Z



# UCC

University College Cork, Ireland  
Coláiste na hOllscoile Corcaigh

# Search for correlations between the optical and radio polarization of active galactic nuclei – I. VLBA polarization data at 15 + 22 + 43 GHz

J. C. Algaba,<sup>1\*</sup> D. C. Gabuzda<sup>1</sup> and P. S. Smith<sup>2</sup>

<sup>1</sup>*Department of Physics, University College Cork, Cork, Ireland*

<sup>2</sup>*Steward Observatory, The University of Arizona, Tucson, AZ 85721, USA*

Accepted 2010 September 7. Received 2010 August 23; in original form 2010 July 7

## ABSTRACT

Although the continua of radio-loud active galactic nuclei (AGNs) are typically dominated by synchrotron radiation over virtually the entire spectrum, it is not clear whether the radio and higher frequency emission originates in the same or different parts of the jet. In some inhomogeneous synchrotron source models, the radio and ultraviolet–optical–infrared emission may be co-spatial, depending on the model parameters considered. Indeed, several different radio–optical correlations based on polarization data have been found recently, suggesting that the optical and radio polarization may be closely related in some AGNs, and that the corresponding emission regions may be co-spatial. Our joint analysis of optical and 15 + 22 + 43 GHz Very Long Baseline Array (VLBA) polarization data for a sample of about 40 AGNs shows that, after correction for the inferred VLBA core Faraday rotations, about 50–55 per cent of BL Lac objects and high-polarization quasars, and about 65 per cent of high-polarization quasars (LPQs) have aligned VLBA-core and optical polarization angles to within 20°; a considerable number of objects also show no obvious relationship between their VLBA-core and optical polarization angles. This may indicate that only some AGNs have co-spatial regions of optical and radio emission in their jets. However, another possibility is that some of the 15–43 GHz VLBA cores have Faraday rotations of the order of several tens of thousand of  $\text{rad m}^{-2}$ , which were not properly fitted using our three-frequency data due to  $n \times \pi$  ambiguities in the observed polarization angles, leading to inaccurate subtraction of the effects of the core Faraday rotation and so incorrect ‘zero-wavelength’ radio polarization angles.

**Key words:** polarization – galaxies: active – galaxies: nuclei – radio continuum: galaxies.

## 1 INTRODUCTION

In general, the ultraviolet–radio (UV–radio) continua of radio-loud active galactic nuclei (AGNs) are dominated by non-thermal synchrotron emission, which is clearly associated with the relativistic jets in these sources. Although synchrotron radiation dominates over essentially the entire spectrum in core-dominated, radio-loud AGNs, it has usually been expected that there should be little correlation between the observed emission in widely spaced wavebands, even if genuinely simultaneous observations are compared. This is partly because early attempts to search for those correlations using integrated measurements were mostly unsuccessful (e.g. Rudnick et al. 1978). In addition, this idea was supported by the fact that optical variations typically occur more rapidly than radio variations, suggesting that the optical emission is generated in a much smaller

volume than the radio emission. Thus, it was considered natural that there be little or no correlation between the high frequency and radio emission in AGNs.

None the less, in some inhomogeneous synchrotron source models for AGN jets, the radio and UV–optical–infrared (UVOIR) emission may be co-spatial, depending on the model parameters considered. Ghisellini, Maraschi & Treves (1985) use a model in which the sources are axially symmetric and collimated. They define co-ordinates  $R$  along the axis and  $r$  in the perpendicular direction, such that

$$r = aR^\epsilon \quad R_0 \leq R \leq R_{\max}, \quad (1)$$

with  $\epsilon \leq 1$ , corresponding in the limiting case to a truncated cone. Similarly, the particle spectrum is assumed to be a single power law up to some maximum energy  $E_{\max} = \gamma_{\max} mc^2$ , such that

$$N(\gamma) = K\gamma^{-s} \quad \gamma \leq \gamma_{\max}. \quad (2)$$

\*E-mail: algaba@physics.ucc.ie

The rest of the dependencies are also taken to have axial dependence on the radial coordinate:

$$B = B_0 \left(\frac{r_0}{r}\right)^m = B_0 \left(\frac{R_0}{R}\right)^{\epsilon m}, \quad (3)$$

$$K = K_0 \left(\frac{r_0}{r}\right)^n = K_0 \left(\frac{R_0}{R}\right)^{\epsilon n}. \quad (4)$$

With those assumptions, the luminosity of the source takes the form

$$L(\nu) = \frac{c_1(\alpha) K_0 B_0^{1+\alpha} \pi a^2 R_0^{1+2\epsilon} \nu^{-\alpha}}{\zeta} \left[ \left(\frac{R}{R_0}\right)^\zeta \right]_{R_1(\nu)}^{R_2(\nu)}, \quad (5)$$

where  $\zeta = 1 + 2\epsilon - \epsilon[n + m(1 + \alpha)]$ ,  $\alpha$  is the spectral index,  $c_1(\alpha_0)$  is a function defined by Blumenthal & Gould (1970), and  $R_1(\nu)$  and  $R_2(\nu)$  are the radii at which the source becomes opaque and the maximum radius contributing at a frequency  $\nu$ , respectively. Thus, depending on the sign of  $\zeta$  (i.e. a particular parametrization of the global geometry of the source), most of the luminosity will be produced either in the inner or in the outer regions of the source. For example, if we have a conical geometry ( $\epsilon = 1$ ) and  $m, n = 2$  (which correspond to conservation of magnetic flux and particle number, respectively), then, above the self-absorption frequency at  $R = R_0$ , the entire spectrum will be dominated by the innermost regions. In practice, this means that observations above that frequency should provide us with information about small inner regions with, in principle, the same properties. Therefore, this provides us with a theoretical basis to look for correlations in the emission in widely spaced bands.

A variety of data have suggested such correlations. For example, Gabuzda, Sitko & Smith (1996) analysed simultaneous optical and 5-GHz very long baseline interferometry (VLBI) polarization measurements for eight AGNs, primary BL Lac objects. Although the results from that study were not conclusive due to the small number of objects considered, there were hints of a correlation between the polarization position angles in the optical and in the VLBI core, with the two nearly always being aligned or orthogonal. This tendency was confirmed later by an analysis of 15 AGNs for which simultaneous optical and 5-GHz data were available (Gabuzda 2003). More recently, Lister & Smith (2000) carried out a joint analysis of Very Long Baseline Array (VLBA) polarization data at 22 and 43 GHz and optical polarization data, with the VLBA and optical data obtained about a month apart. Despite the considerable difference in time between the optical and VLBA measurements, they found clear evidence that the optical polarization ‘knows’ about the radio structure and polarization: the optical polarization angle displayed a tendency to lie along the VLBI jet direction, and the degree of optical polarization was correlated with the core polarization and core luminosity at 43 GHz. Gabuzda et al. (2006) compared simultaneous optical polarization data and 15 + 22 + 43 GHz VLBI polarization data for 11 BL Lac objects and 3C279, with striking results: after correction for Faraday rotation, virtually all the VLBI core polarizations were aligned with the corresponding optical polarization within  $20^\circ$ . The results of Jorstad et al. (2007) at even shorter radio wavelengths show a similar correlation.

Stirling et al. (2003) discovered a long-term tendency for the integrated 1-mm polarization position angle to remain aligned with the innermost 7-mm VLBI jet in BL Lac, even when the inner jet direction varied appreciably. During a more limited period of 1 yr, the optical and 7-mm position angles were also in good agreement. In addition, a remarkable co-rotation of the 7-mm and optical polarization angles of 0420–014 through  $\approx 80^\circ$  over about 10 d was found (D’Arcangelo et al. 2007).

Indications of a connection between  $\gamma$ -ray outbursts and the ejection of VLBI components have also been found. Pohl et al. (1995) reported a major outburst in 0528+174 occurring in Summer 1993 at all frequencies higher than a few GHz, which peaked a few months after a strong outburst in high-energy  $\gamma$ -rays. Jorstad et al. (2001) established a statistical association between the ejection of superluminal radio components and high states of  $\gamma$ -ray emission in compact radio-loud AGNs. These authors concluded that both radio and  $\gamma$ -ray events originate within the same shocked area of the relativistic jet, with this region being near but probably downstream of the core, rather than much closer to the central engine. These collected results provide clear evidence for co-spatiality of the radio and higher energy emission.

However, most of these studies were carried out for so-called blazars, mostly BL Lac objects. Since it is clear that we cannot extrapolate the behaviour of blazars to all kinds of AGNs, we need to observe other types of objects in order to compare their behaviour and check if they follow the same correlation as BL Lac objects. The results of Jorstad et al. (2007) and D’Arcangelo et al. (2007) suggest that some quasars display the same behaviour as BL Lac objects, but the observations of Jorstad et al. (2007) were not strictly simultaneous and the study of D’Arcangelo et al. (2007) involves only one source. In order to expand our analysis, we have analysed multiwavelength data for a total sample of 39 AGNs, including both BL Lac objects and quasars.

In Section 2, we discuss our observations and reduction, and in Section 3, we obtain total, polarized intensity and spectral index distributions for the sources. In Section 4, we search for correlations between the optical and Faraday-corrected radio-core polarization angles and, in Section 5, we summarize our conclusions.

## 2 OBSERVATIONS AND REDUCTION

We obtained new 15 + 22 + 43 GHz VLBA polarization data and nearly simultaneous (within the same day) optical polarization data with the Steward Observatory 2.3-m telescope in three 24-h sessions. The objects selected for our study are 29 AGNs, including BL Lac objects, high-polarization quasars (HPQs) and low-polarization quasars. Here, the degree of polarization refers to the optical band, and the historical dividing line between HPQs and low-polarization quasar (LPQs) is 3 per cent (Moore & Stockman 1984).

### 2.1 VLBA

Polarization observations were carried out in three 24-h sessions on 2004 November 1 (henceforth epoch A, 10 objects), 2005 March 15 (epoch B, 10 objects) and 2005 September 26 (epoch C, 10 objects) at 15, 22 and 43 GHz, respectively, using the NRAO VLBA. In all cases, the sources were observed in a ‘snapshot’ mode, with 8–10 several-minute scans for each object at each frequency spread in time. The resulting coverage in the  $u-v$  (baseline) plane was thus fairly uniform. The total aggregate bit rate used was  $128 \text{ Mbit s}^{-1}$  and the three frequencies observed were 15.285 459, 22.235 459 and 43.135 459 GHz, each of them with two IFs with a bandwidth of 8 MHz. The data reduction and imaging for the radio data were done with the NRAO AIPS (Astronomical Image Processing System) using standard techniques (see e.g. Gabuzda et al. 2006).

The reference antenna used was Los Alamos for epoch A and Fort Davis for epochs B and C. Simultaneous solutions for the instrumental polarizations and source polarizations for the compact sources 1156+295 (epoch A), 0953+254 (epoch B) and 2145+067 (epoch C) were derived using the AIPS task LPCAL.

**Table 1.** Typical beam sizes.

Source [1]	Frequency (GHz) [2]	Beam size (mas) [3]
1637+574	15	$0.88 \times 0.75$
	22	$0.64 \times 0.57$
	43	$0.38 \times 0.28$
1055+018	15	$1.20 \times 0.49$
	22	$1.06 \times 0.37$
	43	$0.39 \times 0.17$

**Table 2.** EVPA corrections.

Epoch [1]	Antenna [2]	15 GHz [3]	22 GHz [4]	43 GHz [5]
A	LA	$94 \pm 4$	$34 \pm 4$	$88 \pm 4$
B	FD	$-50 \pm 4$	$-64 \pm 4$	$35 \pm 4$
C	FD	$-50 \pm 4$	$-64 \pm 4$	$35 \pm 4$

Table 1 shows example beam sizes for a relatively high-declination (1637+574) and low-declination (1055+018) source for 15, 22 and 43 GHz. The beam sizes scale roughly with the frequency in the way expected. The  $u - v$  coverages for sources with similar declinations observed at the three epochs are qualitatively the same, since the ‘snapshot’ observing mode used and the number of sources observed at each epoch were essentially the same.

The absolute calibration of the electric vector position angles (EVPAs) at 22 and 43 GHz was determined using integrated polarization measurements from the NRAO Very Large Array (VLA) polarization and flux monitoring data base.<sup>1</sup> Observations of reasonably compact sources very near in time to our VLBA observations were available for epoch A (2134+004: VLA = 2004 November 1, VLBA = 2004 November 1) and epoch C (2251+158: VLA = 2005 September 25, VLBA = 2005 September 26), but not epoch B. We thus determined the corresponding electric vector position angle (EVPA) calibrations for epochs A and C, and also applied the epoch C calibration for epoch B, having checked for consistency using observations for 0420–014 from the NRAO VLA polarization and flux monitoring data base that were fairly near epoch B in time (VLA = 2005 March 27, VLBA = 2005 March 15). Table 2 summarizes the EVPA corrections that we applied for each of the frequencies at our three epochs. Column [1] shows the epoch, column [2] shows the reference antenna used and columns [3]–[5] show the EVPA corrections applied for 15, 22 and 43 GHz, respectively.

Unfortunately, the NRAO polarization calibration data base does not include measurements at 15 GHz. The University of Michigan Radio Astronomy Observatory monitoring data includes such measurements, but no data were available for any of our objects sufficiently close in time to our VLBI epochs. This situation was saved by the fact that the EVPA correction associated with a particular reference antenna is typically stable over several years or more (Reynolds, Cawthorne & Gabuzda 2001; see also the MOJAVE webpage<sup>2</sup>). We accordingly applied the EVPA corrections for Los Alamos (epoch A) and Fort Davis (epochs B and C) indicated by other polarization experiments surrounding our epochs in time, checking for consistency with MOJAVE images near our epochs.

<sup>1</sup> <http://www.vla.nrao.edu/astro/calib/polar/>

<sup>2</sup> <http://www.physics.purdue.edu/MOJAVE/data.html>

**Table 3.** EVPA corrections at 15 GHz.

Epoch [1]	Exposure [2]	FD [3]	Epoch [4]	Exposure [5]	LA [6]
2003 March 1	BL111F	–51	2002 August 7	BG128A	92
2003 June 15	BL111I	–50	2003 February 5	BL111E	88
2003 August 28	BL111J	–49	2003 March 5	BG128B	96
2005 March 5	BL123C	–50	2004 August 9	BL111N	91
2005 March 15	Epoch B	–50	2004 October 18	BL111P	87
2005 March 23	BL123D	–50	2004 November 1	Epoch A	94
2005 April 21	BL123E	–50	2005 January 6	BL123A	33
2005 May 13	BL123F	–50	2005 September 16	BL123N	90
2005 June 15	BL123I	–47			
2005 July 24	BL123J	–50			
2005 October 29	BL123L	–49			
2005 September 23	BL123O	–50			
2005 September 26	Epoch C	–50			
2005 November 7	BL123P	–49			
2005 December 22	BL123Q	–53			

Table 3 summarizes the EVPA corrections that were found using either Los Alamos (LA) or Fort Davis (FD) as the reference antenna for various independent experiments at 15 GHz. All the EVPA corrections for the various ‘BL’ experiments were taken from the MOJAVE web page. The BG128A and BG128B EVPA corrections are those used to calibrate the data of Gabuzda et al. (2006), based on a joint analysis of VLA and VLBA polarization observations that were separated by only 3 d. Columns [1] and [4] indicate the dates of the observations, columns [2] and [5] indicate the experiments, and columns [3] and [6] indicate the EVPA corrections found for FD and LA, respectively. The corrections we applied to our own experiments at 15 GHz are also given in bold.

Note the striking stability of the corrections over several years. The only exception is the MOJAVE observation obtained on 2005 January 6 (BL123A), when the derived EVPA correction differs from the other values for Los Alamos by about  $60^\circ$ ; the EVPA correction had returned to its former value again by 2005 September. Our epoch A observations were about 2 months before this ‘discrepant’ measurement. We have adopted an EVPA calibration for our epoch A based on the collection of ‘typical’ values for Los Alamos, near  $90^\circ$ , since this value implies polarization structures for the sources observed close to those expected, while the significantly different EVPA calibration for 2005 January 6 implies polarization images that are systematically different from their usual appearance.

After the initial construction of the total intensity maps at 15, 22 and 43 GHz, we used the final self-calibrated visibility data to make maps of the distributions of the Stokes parameters  $Q$  and  $U$  at each frequency. Those maps were used to construct the distribution of polarized flux ( $p = \sqrt{Q^2 + U^2}$ ) and polarization angle ( $\chi = \frac{1}{2} \arctan \frac{U}{Q}$ ), using the AIPS task COMB. We obtained the values of  $\chi$  at specified locations and their errors using the AIPS facility IMSTAT applied to a  $3 \times 3$  pixel region (i.e.  $0.15 \times 0.15 \text{ mas}^2$ , as each pixel corresponds to  $0.05 \text{ mas}$ ) surrounding the location of interest. Since we have VLBA polarization data at three wavelengths, we can derive and correct for the Faraday rotation in the region of the compact radio core.

For the construction of the spectral index maps, we made new versions of the maps using the best-calibrated data but convolving all frequencies with the beam obtained for the 22-GHz map. The 22-GHz beam was chosen as a compromise between the lower (15 GHz) and higher (43 GHz) resolution maps; although we are super-resolving slightly at 15 GHz, this is only by a modest amount.

**Table 4.** Total and polarized intensity properties.

Source	Class	Epoch	$I_{\text{peak}}$ (mJy)			$p$ (per cent)				Spectral index	
			15 GHz	22 GHz	43 GHz	15 GHz	22 GHz	43 GHz	Optical	15–22 GHz	22–43 GHz
[1]	[2]	[3]	[4]	[5]	[6]	[7]	[8]	[9]	[10]	[11]	[12]
0048–097	BL	A	500 ± 30	360 ± 50	290 ± 40	2.3 ± 0.2	2.0 ± 0.4	1.0 ± 0.2	7.8 ± 0.1	−0.51 ± 0.01	−0.32 ± 0.01
0133+476	HPQ	C	1600 ± 210	1500 ± 200	1570 ± 220	2.4 ± 0.4	2.6 ± 0.6	1.6 ± 0.5	7.4 ± 0.3	−0.14 ± 0.01	0.1 ± 0.03
0138–097	BL	C	290 ± 30	270 ± 30	410 ± 50	3.3 ± 0.7	2.1 ± 0.3	3.0 ± 0.6	15.7 ± 0.1	0.05 ± 0.02	−0.04 ± 0.07
0256+075	BL	A	200 ± 10	150 ± 20	170 ± 30	5.2 ± 0.5	7.5 ± 1.3	4.9 ± 1.1	6.7 ± 5.8	−0.2 ± 0.01	−0.01 ± 0.01
0420–014	HPQ	B	4280 ± 200	4060 ± 190	2420 ± 110	1.5 ± 0.1	2.0 ± 0.1	2.5 ± 0.1	5.3 ± 0.5	−0.26 ± 0.03	−0.96 ± 0.02
0745+241	BL	B	600 ± 30	560 ± 30	420 ± 30	1.3 ± 0.1	3.9 ± 0.4	3.8 ± 0.4	17.2 ± 0.3	−0.01 ± 0.01	−0.46 ± 0.01
0804+499	HPQ	A	500 ± 40	400 ± 70	370 ± 60	1.4 ± 0.2	1.4 ± 0.4	0.6 ± 0.3	3.3 ± 0.4	−0.21 ± 0.01	−0.07 ± 0.01
0814+425	BL	C	350 ± 50	310 ± 40	300 ± 30	1.6 ± 0.3	2.0 ± 0.3	3.4 ± 0.6	6.4 ± 0.4	−0.5 ± 0.05	−0.64 ± 0.11
0859+470	LPQ	B	670 ± 40	600 ± 40	370 ± 20	4.1 ± 0.3	4.0 ± 0.3	3.2 ± 0.3	2.2 ± 0.4	−0.25 ± 0.01	−0.74 ± 0.01
0906+430	HPQ	A	600 ± 40	500 ± 60	400 ± 40	0.2 ± 0.1	1.0 ± 0.3	3.5 ± 0.8	10.7 ± 1.2	−0.08 ± 0.01	−0.29 ± 0.01
0953+254	LPQ	B	330 ± 20	390 ± 20	400 ± 20	0.8 ± 0.1	0.5 ± 0.1	2.0 ± 0.2	0.5 ± 0.2	0.38 ± 0.04	−0.12 ± 0.03
1055+018	HPQ	B	3400 ± 130	3570 ± 140	2690 ± 140	4.6 ± 0.3	7.7 ± 0.4	9.2 ± 0.7	13.2 ± 0.4	0.15 ± 0.01	−0.39 ± 0.01
1156+295	HPQ	A	420 ± 30	490 ± 80	530 ± 90	1.2 ± 0.2	2.2 ± 0.5	1.2 ± 0.5	7.6 ± 0.6	0.81 ± 0.02	0.14 ± 0.01
1156+295	HPQ	C	1150 ± 150	1170 ± 140	1210 ± 160	1.4 ± 0.2	1.3 ± 0.2	2.1 ± 0.5	–	0.4 ± 0.02	−0.27 ± 0.05
1510–089	HPQ	B	1130 ± 150	1000 ± 140	670 ± 100	1.7 ± 0.4	1.9 ± 0.4	2.7 ± 0.7	1.7 ± 0.3	−0.22 ± 0.02	−0.46 ± 0.01
1611+343	LPQ	C	1300 ± 330	2270 ± 260	2020 ± 220	0.8 ± 0.3	1.5 ± 0.2	1.4 ± 0.4	0.7 ± 0.2	−0.33 ± 0.03	−0.36 ± 0.02
1633+382	HPQ	A	1340 ± 180	2030 ± 380	1670 ± 220	2.3 ± 0.3	3.8 ± 1.3	4.4 ± 1.3	5.2 ± 0.5	0.1 ± 0.01	−0.36 ± 0.01
1637+574	LPQ	B	820 ± 30	840 ± 30	810 ± 30	1.3 ± 0.1	1.7 ± 0.1	0.5 ± 0.1	0.5 ± 0.2	0.06 ± 0.01	−0.12 ± 0.01
1641+399	HPQ	A	1770 ± 130	1320 ± 230	800 ± 120	2.2 ± 0.3	3.5 ± 0.9	4.6 ± 1.1	6.9 ± 0.3	−0.1 ± 0.01	−0.4 ± 0.01
1652+398	BL	C	440 ± 50	350 ± 30	250 ± 40	2.3 ± 0.4	1.9 ± 0.2	2.1 ± 0.4	0.5 ± 0.1	−0.91 ± 0.05	−0.98 ± 0.08
1739+522	HPQ	B	960 ± 20	800 ± 10	380 ± 4	1.7 ± 0.2	1.3 ± 0.2	1.8 ± 0.1	1.4 ± 0.7	−0.53 ± 0.01	−1.12 ± 0.01
1954+513	LPQ	B	510 ± 20	560 ± 20	380 ± 20	2.2 ± 0.1	3.3 ± 0.2	3.7 ± 0.3	1.1 ± 0.7	0.22 ± 0.02	−0.6 ± 0.01
2134+004	LPQ	A	770 ± 60	610 ± 50	260 ± 30	1.7 ± 0.4	3.2 ± 0.5	1.7 ± 0.3	0.6 ± 0.3	−0.33 ± 0.02	−1.13 ± 0.03
2145+067	LPQ	C	5040 ± 660	4850 ± 460	3600 ± 430	1.4 ± 0.2	2.9 ± 0.4	3.5 ± 0.7	0.1 ± 0.1	−0.3 ± 0.01	−0.59 ± 0.04
2155–152	BL	C	760 ± 70	660 ± 80	580 ± 70	3.4 ± 0.3	4.2 ± 0.8	5.9 ± 1.4	12.7 ± 0.2	−0.02 ± 0.09	0.67 ± 0.08
2230+114	HPQ	A	980 ± 60	1010 ± 130	1340 ± 170	1.3 ± 0.2	2.0 ± 0.6	1.7 ± 0.3	2.0 ± 0.3	0.47 ± 0.01	0.46 ± 0.01
2251+158	HPQ	C	2570 ± 200	4090 ± 420	9740 ± 1080	4.3 ± 0.4	2.9 ± 0.5	2.1 ± 0.6	1.2 ± 0.1	1.7 ± 0.03	2.13 ± 0.07
3C279	HPQ	B	11000 ± 3700	9700 ± 3500	6300 ± 2600	3.7 ± 1.6	1.4 ± 0.6	8.0 ± 3.5	10.0 ± 0.1	−0.12 ± 0.07	−0.28 ± 0.04
OJ287	BL	C	2570 ± 310	2670 ± 320	2490 ± 360	5.0 ± 0.8	4.1 ± 0.6	2.6 ± 0.4	12.9 ± 0.3	−0.19 ± 0.09	0.29 ± 0.02

We then used the task COMB to obtain the spectral index maps after aligning the images using the program developed by Croke & Gabuzda (2008). Some sources had little optically thin jet, making it impossible to determine the shift based on optically thin jet emission. In these cases, we did not apply any shift between the images.

## 2.2 Optical

Nightly optical polarization observations spanning the VLBA observing runs (2004 October 30–November 2; 2005 March 15–17; 2005 September 25–29) were obtained at the Steward Observatory of the University of Arizona. The data were acquired using the SPOL imaging/spectropolarimeter (Schmidt, Stockman & Smith 1992). On various nights, the instrument was configured for either imaging polarimetry using a KPNO ‘nearly Mould’  $R$  filter (6000–7000 Å) or spectropolarimetry using a 600 line  $\text{mm}^{-1}$  diffraction grating. Data acquisition and reduction closely follow those described in Smith et al. (2003, 2007); see also Gabuzda et al. (2006). The spectropolarimetric observations are averaged over the  $R$ -filter bandpass for direct comparison to the imaging polarimetry. A summary of the optical degree of polarization and polarization angles is given in Tables 4 and 5, respectively.

## 3 RESULTS

The objects studied by Gabuzda et al. (2006), which showed a clear correlation between the Faraday-rotation-corrected VLBI core and

optical polarization angles  $\chi$  (i.e. the radio and optical polarization angles were nearly always aligned), were essentially all BL Lac objects (one of which, 1334–127, is taken here to be an HPQ). With our new observations, we expand our analysis to other classes of AGNs, namely HPQs and LPQs. We have new optical+VLBA observations for 29 objects: 15 HPQs, one of which was not detected in our radio observations (0954+556), six LPQs, one of which had very weak optical polarization (2145+067) and eight BL Lac objects. We follow the classifications given in Table 4. Two objects (3C279 and OJ287) were already in the previous sample of Gabuzda et al. (2006), so, in all, we have a total of 39 objects. Hereafter, we will consider this total sample. Where necessary, we will refer to the objects studied in Gabuzda et al. (2006) as belonging to epochs GA (2004 August 7) or GB (2003 March 5).

We summarize our measurements of flux density, degree of linear polarization and spectral index  $\alpha$  ( $S \propto \nu^{1+\alpha}$ ) in Table 4. Columns [1]–[3] show the name of the source, its classification and the epoch at which it was observed. The total intensity peaks in mJy are shown in columns [4]–[6] for the three different frequencies and the polarization percentages are shown in columns [7]–[9]. The total intensity peaks were obtained by applying IMSTAT to a  $3 \times 3$  pixel area at the position of the peak, and the polarization percentages were derived from these values together with the corresponding IMSTAT values for the polarized flux maps. The optical degrees of polarization at our epochs are given in column [10]. The spectral indices in the core region of the sources are shown in column [11] for 15–22 GHz and in column [12] for 22–43 GHz. All uncertainties include both the noise of the map and the root mean square (rms)

**Table 5.** Values of radio-core  $\chi$ .

Source [1]	Class [2]	Epoch [3]	$\chi_{15\text{GHz}}$ [4]	$\chi_{22\text{GHz}}$ [5]	$\chi_{43\text{GHz}}$ [6]	RM [7]	rms [8]	$\chi_0$ [9]	$\chi_{\text{Opt}}$ [10]	$\Delta\chi$ [11]
OJ287	BL	C	$-41 \pm 4$	$-20 \pm 4$	$-3 \pm 6$	$-1920 \pm 120$	0.9	$1 \pm 2$	$-67 \pm 1$	68
		GB	$3 \pm 5$	$-10 \pm 3$	$-7 \pm 3$	–	–	$-7 \pm 3$	$-10 \pm 15$	3
3C279	HPQ	B	$-3 \pm 4$	$10 \pm 3$	$16 \pm 5$	$-1020 \pm 110$	0.8	$20 \pm 2$	$68 \pm 1$	48
		GB	$5 \pm 4$	$35 \pm 4$	$51 \pm 4$	$-2360 \pm 120$	1.0	$58 \pm 2$	$55 \pm 1$	3
0048–097	BL	A	$134 \pm 5$	$118 \pm 6$	$106 \pm 6$	$1450 \pm 50$	0.4	$102 \pm 1$	$66 \pm 1$	36
0133+476	HPQ	C	$-114 \pm 3$	$-116 \pm 3$	$-118 \pm 4$	$200 \pm 30$	0.2	$-118 \pm 0$	$-177 \pm 1$	59
0138–097	BL	C	$-112 \pm 5$	$-64 \pm 6$	$-24 \pm 4$	$-4560 \pm 260$	2.1	$-13 \pm 4$	$-9 \pm 1$	4
0256+075	BL	A	$40 \pm 4$	$25 \pm 4$	$38 \pm 4$	$200 \pm 820$	6.0	$32 \pm 12$	$92 \pm 25$	60
0420–014	HPQ	B	$126 \pm 4$	$126 \pm 5$	$120 \pm 5$	$270 \pm 200$	1.5	$121 \pm 3$	$78 \pm 3$	43
0745+241	BL	B	$73 \pm 4$	$88 \pm 5$	$108 \pm 4$	$-1780 \pm 320$	2.6	$111 \pm 5$	$60 \pm 1$	51
0804+499	HPQ	A	$39 \pm 4$	$1 \pm 5$	$-68 \pm 60$	$3370 \pm 530$	14.5	$-35 \pm 10$	$-14 \pm 4$	21
0814+425	BL	C	$-335 \pm 4$	$-140 \pm 4$	$14 \pm 6$	$-17\,800 \pm 1000$	7.5	$52 \pm 15$	$117 \pm 2$	65
0823+033	BL	GB	$30 \pm 3$	$32 \pm 4$	$41 \pm 4$	–	–	$41 \pm 4$	$68 \pm 3$	27
0859+470	LPQ	B	$38 \pm 4$	$40 \pm 4$	$46 \pm 7$	$-350 \pm 170$	1.3	$45 \pm 3$	$46 \pm 6$	1
0906+430 <sup>b</sup>	HPQ	A	$-526 \pm 5$	$-250 \pm 6$	$-54 \pm 5$	$-24\,440 \pm 470$	3.7	$11 \pm 7$	$19 \pm 3$	8
0953+254	LPQ	B	$-110 \pm 3$	$-33 \pm 3$	$16 \pm 4$	$-6550 \pm 50$	0.4	$35 \pm 1$	$-1 \pm 15$	36
1055+018	HPQ	B	$145 \pm 5$	$147 \pm 5$	$147 \pm 4$	$-100 \pm 50$	0.3	$148 \pm 1$	$132 \pm 1$	16
1147+245	BL	GB	$26 \pm 6$	$74 \pm 3$	$74 \pm 3$	–	–	$74 \pm 3$	$59 \pm 2$	15
1156+295	HPQ	A	$46 \pm 5$	$-10 \pm 4$	$-49 \pm 40$	$4830 \pm 40$	0.7	$-60 \pm 1$	$-115 \pm 7$	55
1334–127	HPQ <sup>c</sup>	GB	$48 \pm 5$	$38 \pm 3$	$45 \pm 3$	–	–	$45 \pm 3$	$48 \pm 12$	3
1418+546	BL	GA	$129 \pm 5$	$123 \pm 6$	$31 \pm 4$	$410 \pm 60$	0.5	$30 \pm 1$	$23 \pm 2$	7
1510–089	HPQ	B	$53 \pm 3$	$58 \pm 4$	$55 \pm 8$	$-270 \pm 200$	1.8	$59 \pm 4$	$50 \pm 5$	9
1538+149	BL	GB	$-34 \pm 3$	$-44 \pm 3$	$-37 \pm 3$	–	–	$-37 \pm 3$	$-32 \pm 3$	5
1611+343	LPQ	C	$-32 \pm 8$	$-11 \pm 3$	$4 \pm 8$	$-1860 \pm 70$	0.4	$9 \pm 1$	$-20 \pm 6$	29
1633+382	HPQ	A	$20 \pm 4$	$20 \pm 4$	$32 \pm 4$	$-570 \pm 430$	3.2	$31 \pm 6$	$60 \pm 2$	29
1637+574	LPQ	B	$-41 \pm 5$	$-34 \pm 9$	$-31 \pm 5$	$-520 \pm 40$	0.4	$-29 \pm 1$	$-36 \pm 10$	7
1641+399	HPQ	A	$68 \pm 4$	$65 \pm 6$	$85 \pm 5$	$-760 \pm 670$	5.5	$83 \pm 10$	$78 \pm 1$	5
1652+398	BL	C	$171 \pm 5$	$-20 \pm 9$	$-166 \pm 6$	$17420 \pm 500$	4.7	$-211 \pm 8$	$-133 \pm 3$	78
1739+522	HPQ	B	$-70 \pm 4$	$-61 \pm 3$	$-55 \pm 4$	$-780 \pm 3$	0.1	$-53 \pm 0$	$-67 \pm 14$	14
1749+096	BL	GA	$46 \pm 4$	$18 \pm 4$	$-10 \pm 4$	$2860 \pm 290$	2.5	$-16 \pm 4$	$1 \pm 1$	17
1823+568	BL	GA	$37 \pm 4$	$37 \pm 4$	$30 \pm 4$	$400 \pm 100$	1.9	$30 \pm 3$	$-24 \pm 2$	54
1954+413	LPQ	B	$-449 \pm 4^a$	$-203 \pm 3^a$	$-69 \pm 3$	$-24\,400 \pm 640$	5.2	$2 \pm 8$	$6 \pm 20$	4
2131–021	BL	GA	$78 \pm 6$	$82 \pm 5$	$80 \pm 5$	$-100 \pm 180$	1.3	$81 \pm 2$	$151 \pm 12$	70
2134+004 <sup>b</sup>	LPQ	A	$427 \pm 13$	$180 \pm 9$	$40 \pm 8$	$20\,000 \pm 900$	6.3	$-19 \pm 10$	$-18 \pm 16$	1
2155–152	BL	C	$14 \pm 9$	$22 \pm 5$	$39 \pm 4$	$-1450 \pm 500$	3.6	$41 \pm 5$	$55 \pm 1$	14
2200+420	BL	GA	$140 \pm 5$	$63 \pm 4$	$23 \pm 5$	$6100 \pm 370$	2.9	$4 \pm 5$	$5 \pm 1$	1
2230+114	HPQ	A	$430 \pm 5$	$214 \pm 4$	$47 \pm 4$	$19\,800 \pm 900$	6.8	$-2 \pm 13$	$-32 \pm 4$	30
2251+158	HPQ	C	$-47 \pm 4$	$-65 \pm 4$	$-72 \pm 4$	$1320 \pm 170$	1.3	$-77 \pm 2$	$-131 \pm 2$	54
2254+074	BL	GA	$64 \pm 5$	$53 \pm 5$	$48 \pm 6$	$820 \pm 90$	0.6	$45 \pm 1$	$43 \pm 1$	2

<sup>a</sup>This angle was rotated by  $90^\circ$  before calculating the RM.

<sup>b</sup>There is uncertainty about the presence of an optical-depth transition in our observed frequency range.

<sup>c</sup>Also sometimes classified as a BL Lac object

deviation of the quantity, obtained by applying the AIPS procedure IMSTAT to a  $3 \times 3$  area around the location of interest. Both the optical and radio degrees of polarization have been corrected for statistical bias in accordance with the prescription of Wardle & Kronberg (1974). This made little difference in the vast majority of the measurements, since this correction is significant only for measurements with signal-to-noise ratios of up to a few.

Intensity, polarization and spectral index maps are presented in Algaba (2010). An example of these maps is given in Fig. 1. In the top and middle panels, the contours show the total intensity and the sticks of the EVPAs, with the length of the sticks being proportional to the degree of polarization. The beam used is shown in the bottom left-hand corner of each image. The bottom panels are the spectral index maps taken from 15 to 22 GHz (left-hand side) and from 22 to 43 GHz (right-hand side). The interested reader can contact J. C. Algaba for intensity, polarization and spectral index maps of the other sources.

### 3.1 Core spectral indices

It is widely accepted that the emission of core-dominated AGNs is dominated by synchrotron radiation over a wide range of frequencies from radio to optical wavelengths and sometimes even further, to X-rays. The very detection of highly polarized optical emission demonstrates a substantial contribution from synchrotron radiation. The optical radiation is always optically thin, whereas, in the radio, we can have several possibilities: a region in the source can be optically thin, optically thick or undergo an optical-depth transition at the observed frequencies.

This means that we can find a great variety of behaviours with regard to the intensity at different radio frequencies. Although most of the VLBI cores (about 22 of 29) are either predominantly or partially optically thin at all three frequencies observed (i.e.  $\alpha$  is negative, up to values close to zero), there are others in which the spectral indices suggest that there may be an optical-depth transition

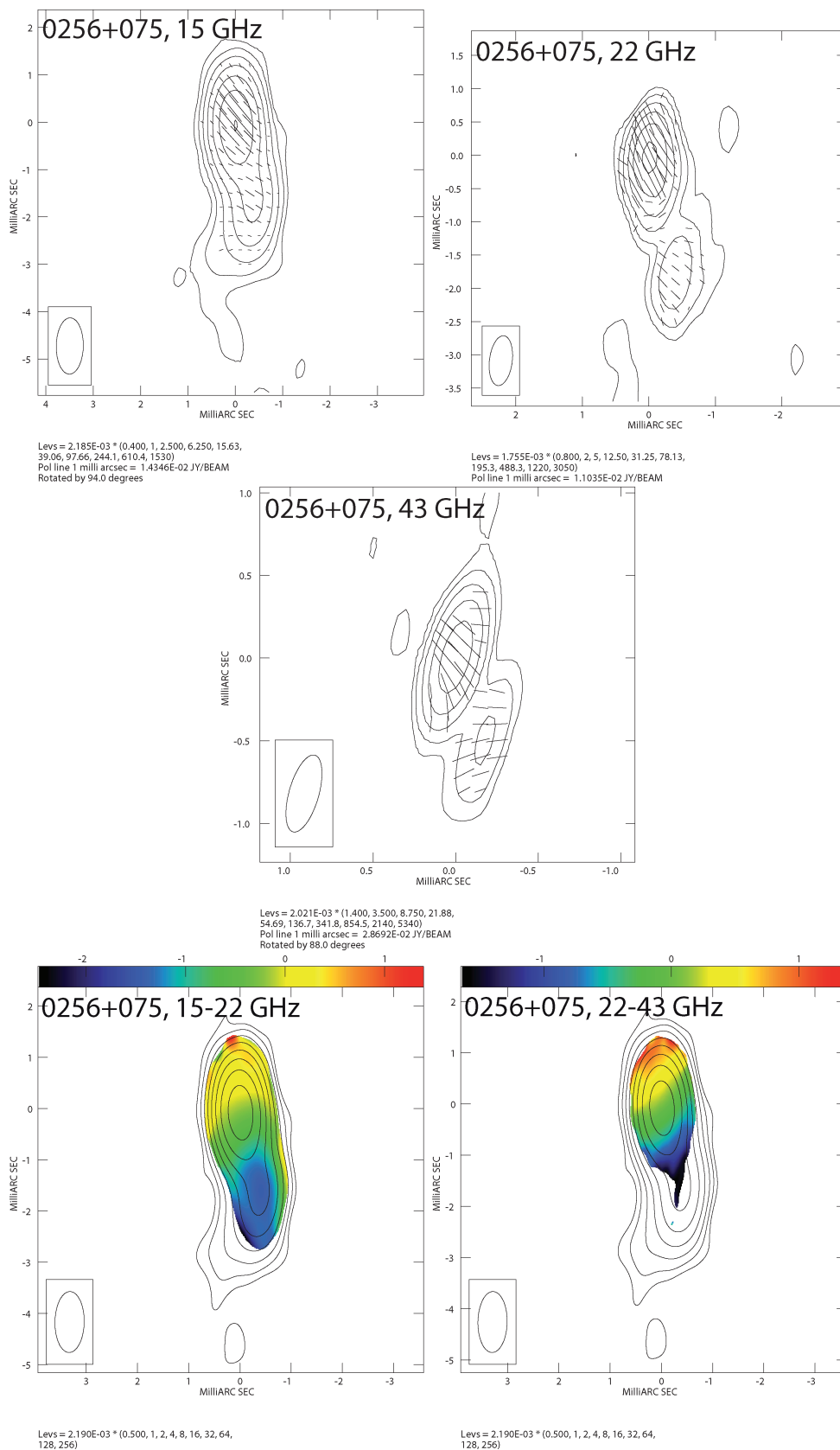


**Figure 1.** 0256+075. Top and middle panels: polarization maps for 15, 22 and 43 GHz. Bottom panel: spectral index maps for 15–22 and 22–43 GHz. Contours are as follows (in mJy): 15 GHz: 0.43, 0.87, 2.19, 4.37, 34.15, 85.35, 213.39; 22 GHz: 1.4, 3.51, 8.78, 21.94, 54.84, 133.61; 43 GHz: 2.83, 7.07, 17.68, 44.22, 110.53; and spectral index maps: 1.1, 2.19, 4.38, 8.76, 17.52, 35.04, 70.08, 140.16.

(0953+254, 1055+018, 1156+295 at epoch C and 1954+513) and a few that seem to be optically thick even at the highest observed frequencies (2230+114 and 2251+518). We will take the inferred optical depth for the VLBI core (thin or thick) into account below when comparing the observed optical and zero-wavelength VLBI polarization angle.

### 3.2 Observed core polarization

Synchrotron radiation can give rise to a degree of polarization up to 75 per cent, when the distribution of electron pitch angles is random and the magnetic field is perfectly ordered (Pacholczyk 1970). However, it is rare to observe such high degrees of polarization. At least two effects are contributing: integration over an extended emission region and the incoherent sum of different polarization orientations over a set of layers or regions in the source. As a result, the observed degree of polarization in the cores decreases appreciably to values typically no higher than  $\simeq 5$  per cent. Due to the nature of Faraday rotation, which is dependent on the square of the wavelength, the sum of different polarized components will be less coherent for lower frequencies, which can cause the observed degree of polarization to increase with frequency. Also, other physical conditions, such as an optical depth transition, blending with the inner jet or the degree of ordering of the magnetic field, can have important effects on the degree of polarization.

In our sample, about 10 sources have degrees of polarization that increase with frequency. Others show some evidence for a maximum (0256+075, 1156+295 at epoch A, 1637+574, 2134+004) or a minimum (0138–097, 3C279) of the degree of polarization around 22 GHz. A few sources also have a degree of polarization which decreases with frequency (0048–097, 0859+470, 2251+158 and OJ287). Finally, the degrees of polarization for some sources are essentially the same at all three frequencies within their  $1\sigma$  errors. The only one for which it may be possible to relate a change in the degree of polarization with an optical depth transition is 0953+254, which appears to have a spectral peak near 22 GHz and has a core degree of polarization of about 0.5–0.8 per cent at 15 and 22 GHz, which increases to more than 2 per cent at 43 GHz.

## 4 SEARCH FOR EVPA CORRELATIONS

We obtained the EVPA in the core regions of the sources using the AIPS procedure IMSTAT for all three radio frequencies. For this, we selected  $3 \times 3$  pixel areas. The uncertainty for each angle was taken to be the sum of the rms deviations given by IMSTAT associated with that region and the EVPA calibration uncertainty added in quadrature. The EVPA estimates were obtained as close to the VLBA core as possible, either in the core itself or in the innermost jet (when the core polarization was weak). For consistency, we checked several nearby regions to make sure the EVPA was stable over an appreciable region around the selected  $3 \times 3$  area. Note that, as the optical polarization of 2145+067 is very low, compatible with zero (see Table 4), we will not include this source in our following analysis.

Table 5 summarizes these results. Columns [1]–[3] are as in Table 4. Columns [4]–[6] show the polarization angles  $\chi$  in degrees at each of the observed frequencies. Columns [7]–[9] indicate the result of our linear Faraday-rotation fits, that is, the rotation measures (RMs) in  $\text{rad m}^{-2}$ , the rms deviations for the observed EVPAs from the fit in degrees and the zero-wavelength intrinsic EVPA  $\chi_0$ . In column [10], the optical  $\chi_{\text{opt}}$  is given and, in column [11], the difference  $\Delta\chi = |\chi_{\text{opt}} - \chi_0|$ . The errors in the RMs and  $\chi_0$  values

were obtained by using standard linear-fitting procedures, taking into account the individual errors of the EVPAs used for the fit.

Note that we obtained the EVPA values close to the peak emission, which is usually essentially coincident with the  $\tau = 1$  surface, although this is not always true. Thus, caution must be taken when identifying the polarization angle of the VLBA core with the polarization angle of the real  $\tau = 1$  surface.

We discussed above the presence of small shifts between the images at different radio frequencies; this is due to the frequency dependence of the position of the VLBI core (Königl 1981). If we wish to directly compare the optical and radio core polarization angles, we must estimate the magnitude of this core shift between our radio frequencies and the optical. Kovalev et al. (2008) estimated that the core shift between 8.6 GHz and the optical is about 0.1 mas. We estimate that the core shifts between 15 GHz and the optical are about the same order of magnitude as the core shift between our two closest frequencies (i.e. less than 0.05 mas for most of our sources and in no case higher than 0.1 mas). We thus conclude that the core shift has no important effects on our calculations of the radio and optical  $\chi$ .

To ensure a more accurate comparison of the core–region and optical polarization angles, we jointly considered the core spectral indices and EVPAs of the sources in our sample (see Table 4). Several of the objects display signs of an optically thick–thin transition in the VLBI core in our frequency range. These sources showed jumps of roughly  $90^\circ$  between the polarization angles at neighbouring frequencies, as well as spectral indices that suggest a thin–thick transition. In the case for which we felt most confident, 1954+513 (see Table 4), we rotated the inferred optically thick core polarization angles by  $90^\circ$  at 15 and 22 GHz (marked in Table 5) before comparison with the optically thin polarization angle (43 GHz). Theoretically, we might expect a decrease in the degree of polarization by about a factor of 5–7 in the transition from the optically thin to thick regime (Pacholczyk 1970), whereas we observe a decrease only by a factor of 1.5. Gabuzda & Gómez (2001) report a similar ratio of the observed core polarizations at 22 and 5 GHz ( $m_{22}/m_5 \simeq 1.7$ ) for observations in which the VLBI core was interpreted as being optically thin at 22 GHz but optically thick at 5 GHz. It is possible that this deviation from the theoretically expected behaviour is due at least in part to the fact that we are not observing a homogeneous region.

There are also two sources (0906+430 and 2134+004) that display only tentative evidence for optical-depth transitions. For these objects, either the evidence for a transition is not clear or a comparison of the values of  $\chi$  at different wavelengths and the spectral indices provide contradictory information. Those cases are also indicated in Table 5.

We fitted VLBA core EVPAs with a linear dependence on the wavelength squared, as expected for external Faraday rotation:  $\chi = \chi_0 + (\text{RM})\lambda^2$ . There is, of course, an intrinsic ambiguity in the polarization angles, since the polarization plane remains unaltered, if the EVPA is rotated by an integer number of  $\pi$ ,  $\chi = \chi + n\pi$ ,  $n = \pm 1, \pm 2, \pm 3, \dots$ . In some cases, we believe it was necessary to make use of this ambiguity to obtain the true angles and RMs. For example, in 2230+114, the nominal observed EVPAs are  $70^\circ$ ,  $34^\circ$  and  $47^\circ$  at 15, 22 and 43 GHz, respectively. Clearly, this does not yield the  $\lambda^2$  behaviour expected for Faraday rotation. However, rotating the 22-GHz EVPA by  $\pi$  and the 15-GHz EVPA by  $2\pi$  yields a good  $\lambda^2$  fit corresponding to the Faraday RM indicated in Table 5. Although it is impossible to be sure of these rotations when we have measurements at only three frequencies, we believe that this likely represents a correct fit for this particular core RM.



There were six such cases, which can be identified as those whose RMs exceed a few thousand  $\text{rad m}^{-2}$ . The 15- and 22-GHz values of  $\chi$  were rotated by up to  $2\pi$  only when these small adjustments to the observed EVPAs produced much improved RM fits, similar to the case of 2230+114 described above. We note here that such relatively large RMs would in the simplest case be expected to give rise to appreciable beam depolarization at our lower frequencies, in accordance with the relation  $m(\lambda) = m_0 \|\sinh(\text{RM} \lambda^2)\|$ , where  $m_0$  is the degree of polarization that would be observed in the absence of Faraday depolarization. This type of simple behaviour is not obviously displayed by the cores we propose to have relatively high RMs. Similarly, no simple depolarization pattern was displayed by the core RM values derived by Zavala & Taylor (2004): the range of observed core degrees of polarization at 8 and 15 GHz is virtually identical, and a wide range of ratios of the 8- and 15-GHz core polarizations are observed, including cases where the observed polarization angles give a good  $\lambda^2$  fit, but the observed core polarization at 8 GHz exceeds that at 15 GHz. Therefore, we feel that this likely reflects the fact that we are dealing with a somewhat inhomogeneous core region, rather than arguing against the possibility that these cores are subject to relatively high external Faraday rotation (for example, the decrease in polarization due to beam depolarization at lower frequencies may be balanced by an increase in the contribution to the total observed ‘core’ polarization from the inner jet at these frequencies).

Our results are shown in the  $\chi$  versus  $\lambda^2$  plots in Figs 2–5, where the optical polarization angle has also been included as the leftmost point in the figures at zero wavelength. Note that this optical point was not included when obtaining linear fits for the radio polarization angles. Most of the sources show acceptable  $\lambda^2$  fits for their EVPAs, with either the nominal observed EVPA values or by taking into account modest rotations by  $\pm\pi$  or  $\pm 2\pi$  as described above, while a few do not. In some cases, the optical polarization angles shown at zero wavelength are consistent with the  $\lambda^2$  fits for the radio polarization angles (e.g. 0138–097, 0859+470, 0906+430, 1954+413, 2134+004), while in many cases they are not. We consider various possible reasons for these results below.

A few cases require additional comments. (i) 0906+430 has very little change in its spectral indices between 43 and 22 GHz and between 22 and 15 GHz, but the large jump between  $\chi_{15\text{GHz}}$  and  $\chi_{22\text{GHz}}$  seems to indicate either that an optical-depth transition occurs between 15 and 22 GHz or that the core has a high Faraday rotation. Based on its spectral index, we decided the second option to be more physical. (ii) As noted above, 1954+413 shows a smooth rotation of its values of  $\chi$ , but its spectral indices suggest that there may be an optical-depth transition. We accordingly rotated  $\chi_{22\text{GHz}}$  and  $\chi_{15\text{GHz}}$  by  $90^\circ$ . At this point we observed that we could obtain a good  $\lambda^2$  fit by adding  $\pi$  rad to  $\chi_{15}$ , which implied both an optical transition and a high RM. (iii) 2134+004 appears to be optically thin at every radio wavelength, although the fit is much better if  $\chi_{15\text{GHz}}$  and  $\chi_{22\text{GHz}}$  are both rotated by  $90^\circ$ . Another option that we consider more likely is that this source likewise shows high RM. (iv) The case of 1510–089 is particularly interesting: an accurate  $\lambda^2$  fit can be traced from  $\chi_0$  to  $\chi_{22\text{GHz}}$ , but  $\chi_{15\text{GHz}}$  lies off the fit. This could be explained if, at this long wavelength, some other polarization components are being blended into the beam. Although the VLBA images do not rule this out, we cannot confirm this based on our current data.

Nearly all the VLBA radio-core EVPAs follow the expected  $\lambda^2$  dependence within the errors. Yet, although we might expect from the previous results of Gabuzda et al. (2006) that the optical EVPA should also follow the same fit, this is usually not the case. The

optical and radio core values of  $\chi$  for the BL Lac objects are often aligned, but sometimes misaligned.

Fig. 6 shows the distribution of  $\Delta\chi$  for the total sample of 39 objects. Note that 3C279 and OJ287 have been included twice, since they were also observed by Gabuzda et al. (2006) and show appreciably different behaviour at the two epochs. We find two groups of sources: one group with  $\Delta\chi \sim 0^\circ$  and another with  $\Delta\chi \sim 55^\circ$ . The first group of sources can be explained if the radio and optical polarized emission is approximately co-spatial. The second group, showing a possible peak with  $\Delta\chi \sim 55^\circ$ , is puzzling.

The BL Lac objects (white) show a clear peak near  $\Delta\chi \sim 0^\circ$  and a possible second peak near  $\Delta\chi \sim 55^\circ$ – $60^\circ$ . The LPQs (light grey) also show a peak near  $\Delta\chi \sim 0^\circ$ , whereas the HPQs (dark grey) show a flatter distribution.

#### 4.1 The optical and VLBI core polarization angles

A Kolmogorov–Smirnov test indicates that, if the distributions of  $\Delta\chi$  for the BL Lacs and quasars were empirically the same, then there would be a 40 per cent chance of the data being distributed as they are. This clearly shows that there is currently no evidence that the BL Lacs and quasars show different  $\Delta\chi$  distributions.

The simplest explanation for an arbitrary offset between the VLBI core and optical polarization angles is that the optical and radio emission comes from different regions with different magnetic field directions. However, in this case, we would not expect any peaks in the  $\Delta\chi$  distribution.

One way to explain the peak around  $\Delta\chi \sim 50^\circ$  could be if these VLBI cores are undergoing internal Faraday rotation (Burn 1966). In the case of internal Faraday rotation, for wavelengths long enough, the wavelength dependence of the observed values of  $\chi$  deviates from a ‘ $\lambda$ -squared’ law and the observed values of  $\chi$  oscillate around some value near  $45^\circ$ . Thus,  $\chi$  measurements at several wavelengths in this regime would yield spurious Faraday RMs, implying an incorrect zero-wavelength  $\chi$  that is roughly  $45^\circ$  from the true value. We consider this possibility in Section 4.4. It is possible for some sources that, despite showing a misalignment between the optical and radio-core polarization angles, the optical and radio emission is closely related. This was inferred previously for OJ287 (Gabuzda et al. 1996), which displayed  $\Delta\chi \sim 40^\circ$ , but showed evidence that the radio and optical values of  $\chi$  rotated together over  $\sim 1$  yr. Unfortunately, in our expanded sample, we only observed two sources at two different epochs. In OJ287,  $\chi_0$  and  $\chi_{\text{opt}}$  are aligned at one epoch but roughly perpendicular at the other; the radio and optical values of  $\chi$  for 3C279 are similarly aligned at one epoch and misaligned at the other.

It is possible that, in some sources, the misalignment comes from complex spatial structure in the radio-core polarization. In those cases, we could obtain dissimilar values for  $\chi$  by analysing different nearby regions in the vicinity of the VLBA core. Thus, the intrinsic  $\chi_0$  and  $\Delta\chi$  values obtained for those sources could be unreliable. To investigate this possibility, we searched the sample for sources showing complex spatial behaviour of  $\chi$  in their cores. We found that this may be the case for 0138–097, 0804+499, 0906+430, 1156+295, 1510–089, 1611+343, 1637+574, 1652+398 and 3C279. Fig. 7 shows a histogram analogous to Fig. 6 but without these sources. It is clear that the overall shape of the  $\Delta\chi$  distribution has not significantly changed, indicating that the complex core polarization structure does not seem to be the cause of the misalignments between the optical and radio polarization angles.

Another possibility is that, due to time variability, we are not properly matching the optical and radio-core polarization angles.

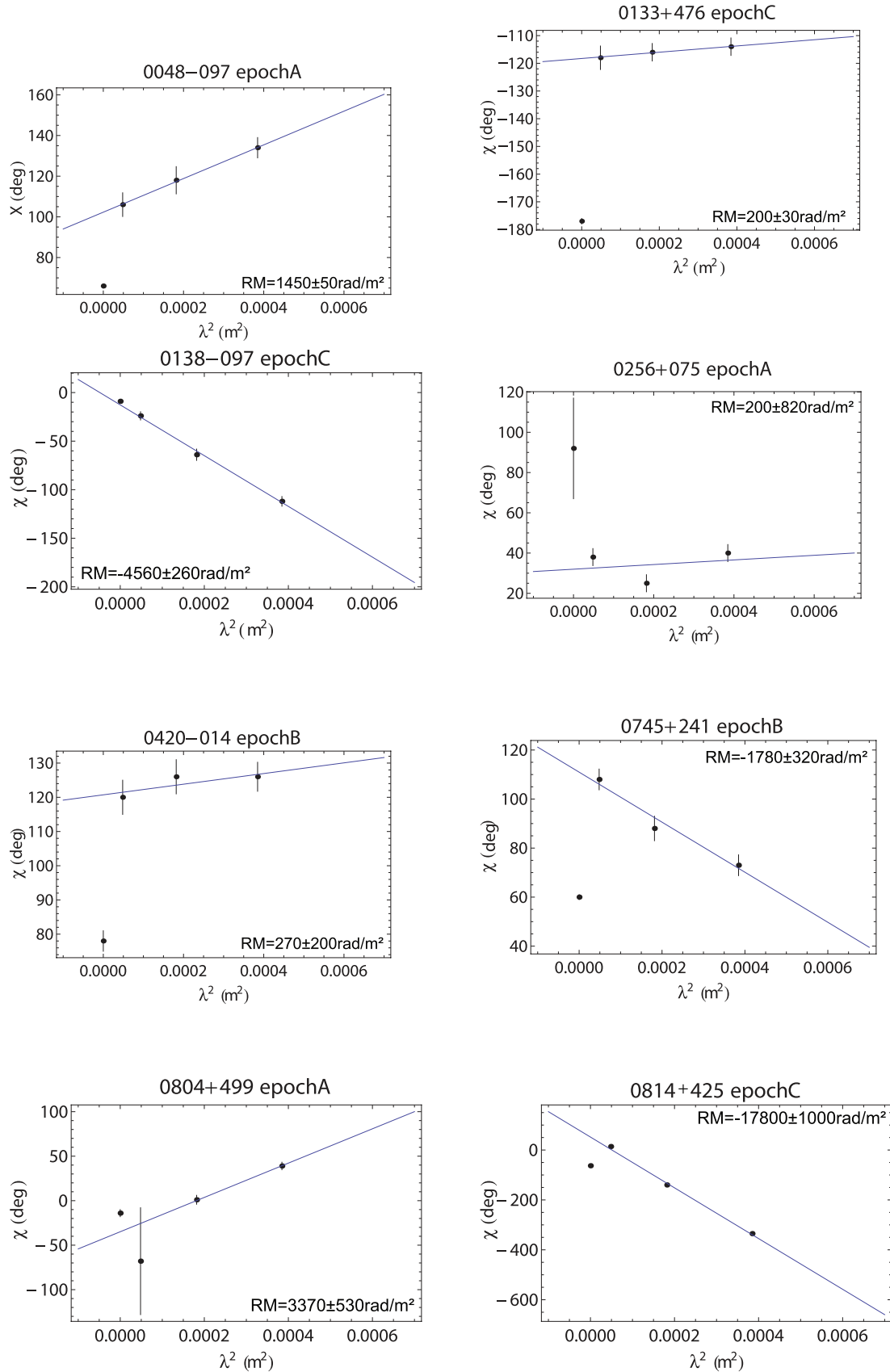


**Figure 2.** Rotation measurements for radio wavelengths and optical EVPA for comparison: 0048–097, 0133+476, 0138–097, 0256+075, 0420–014, 0745+241, 0804+499 and 0814+425.

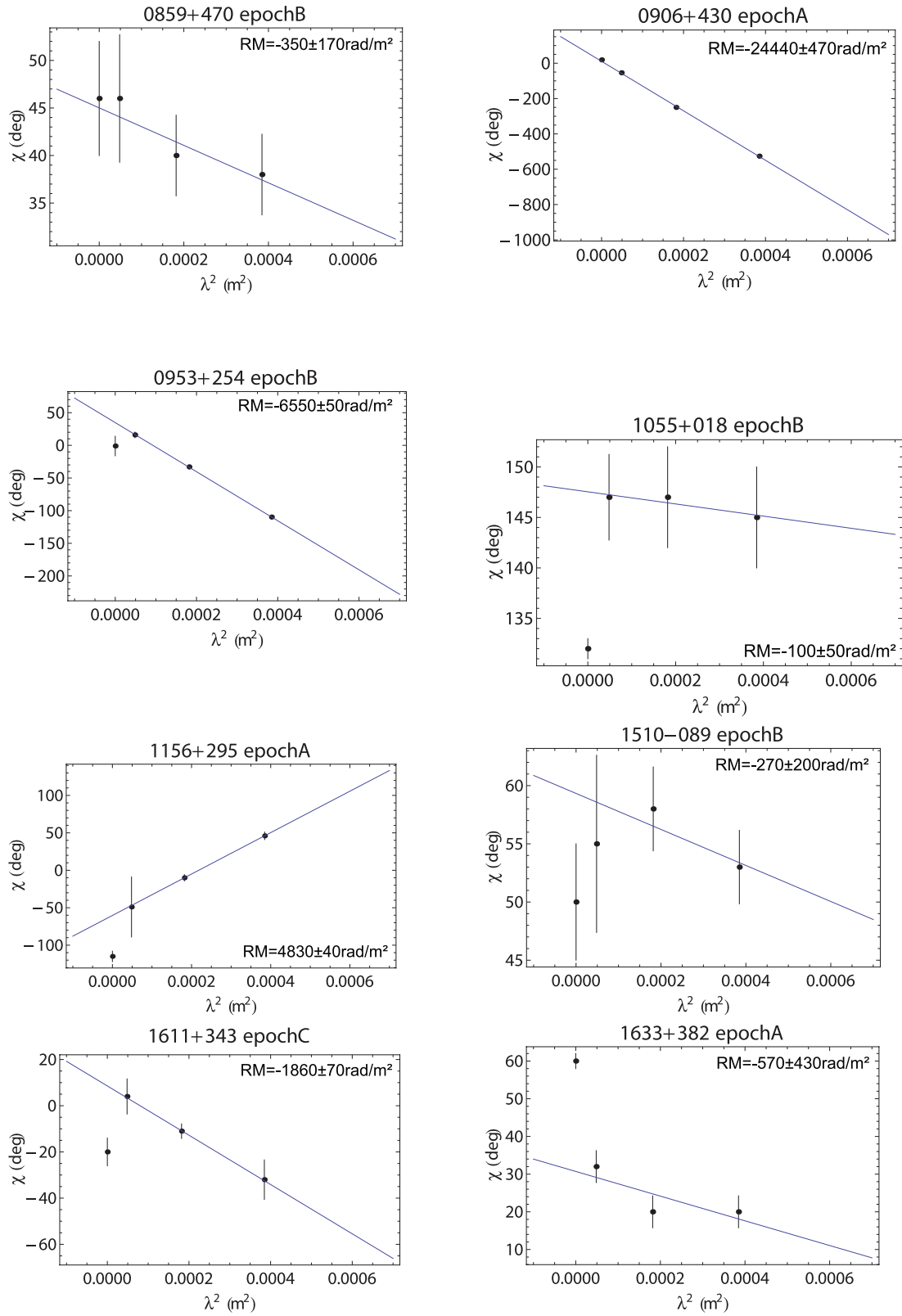


**Figure 3.** Rotation measurements for radio wavelengths and optical EVPA for comparison: 0859+470, 0906+430, 0953+254, 1055+018, 1156+295, 1510-089, 1611+343 and 1633+382.

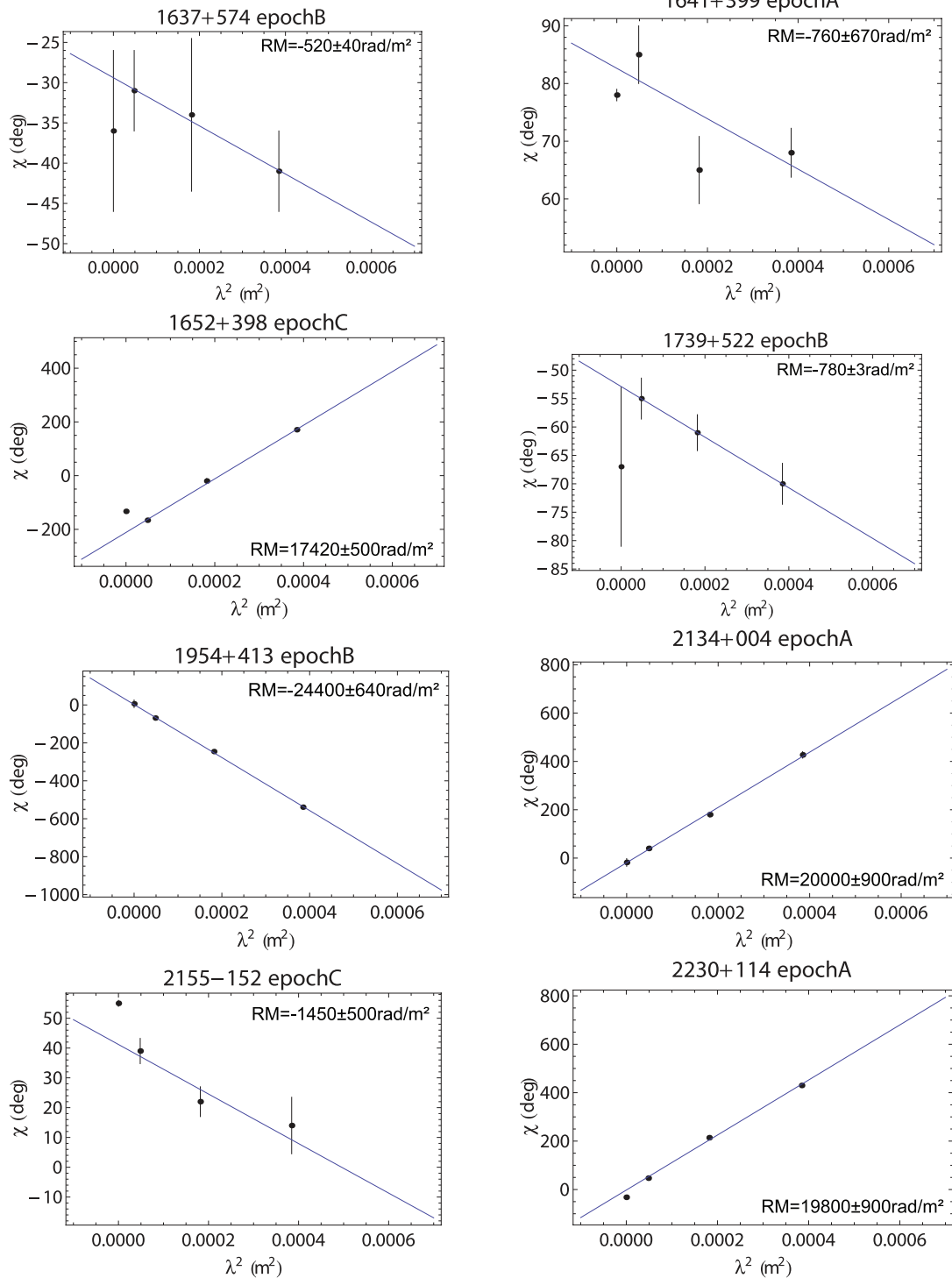


**Figure 4.** Rotation measurements for radio wavelengths and optical EVPA for comparison: 1637+574, 1641+399, 1652+398, 1739+574, 1954+413, 2134+004, 2155–152 and 2230+114.

However, there are several reasons why we feel that this is unlikely. First, the optical polarization angles were tracked over several days and little variability was found. Since the variability time-scale typically increases with decreasing frequency, this makes it very unlikely that there was rapid variability in the radio during our observations, since the optical and radio observations were simultaneous to within a day.

The observed optical polarization in some of the LPQs may not be associated with synchrotron emission from the jet; however, this would not lead to peaks in the  $\Delta\chi$  distribution, whereas four out of six LPQs have  $\Delta\chi \leq 10^\circ$ . Of course, if significant polarization variability is observed in an LPQ, then the source of optical polarized flux must be synchrotron radiation, as it is with the BL Lacs and HPQs.

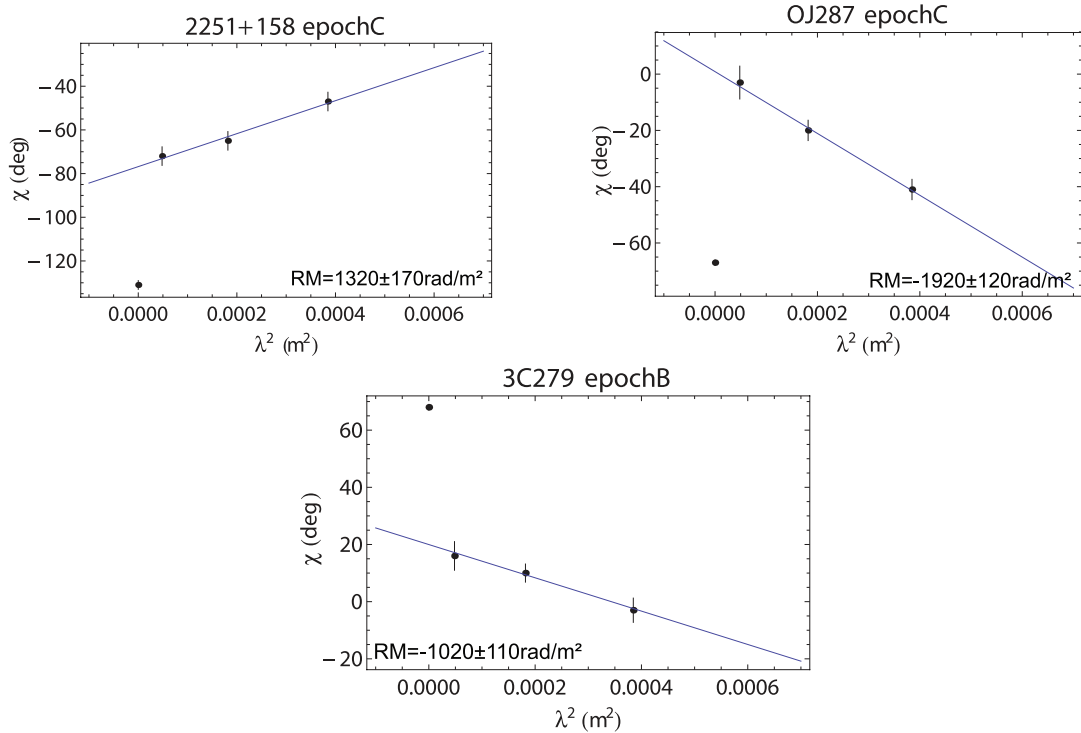


**Figure 5.** Rotation measurements for radio wavelengths and optical EVPA for comparison: 2251+158, OJ287 and 3C279.

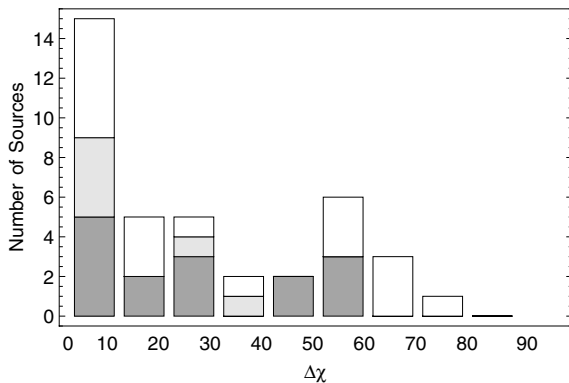


**Figure 6.** Histogram of the difference between the radio-core and optical polarization angles, including the sources in Gabuzda et al. (2006) and in our sample, including BL Lac objects (white), HPQs (dark grey) and LPQs (light grey).

It seems physically reasonable that some kind of correlation between  $\Delta\chi$  and the degree of polarization in the core may exist. High degrees of polarization reflect a high degree of order and uniformity of the magnetic field, giving rise to well-defined values of  $\chi$  over potentially a wide range of frequencies. On the other hand, low degrees of polarization indicate the presence of tangled magnetic fields or depolarization, giving rise to more uncertain values of  $\chi$ . To check this possibility, we obtained the degrees of polarization in the regions where the values of  $\chi$  were obtained and compared them with the inferred  $\Delta\chi$  values. The results are shown in Fig. 8. From the figures, it is clear that both the degree of polarization and the scatter of this quantity (i.e. the standard deviation around the average) increase with frequency. However, in none of the cases does a correlation with  $\Delta\chi$  appear. This is true for both the data for individual classes and the combined data as a whole. Thus, we find

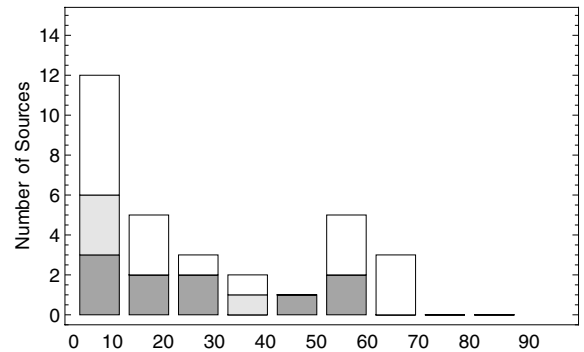


**Figure 7.** Histogram of the difference between the radio- and the optical-core polarization angles, when sources with complex spatial radio core polarization angle are not included. BL Lac objects (white), HPQs (dark grey) and LPQs (light grey).

no evidence for a correlation between  $\Delta\chi$  and different degrees of polarization in the cores of the observed sources.

#### 4.2 Correlation with jet direction

It is known that the Faraday-corrected radio-core polarization angles tend to be either parallel or perpendicular to the jet direction  $\Theta_j$  (e.g. Gabuzda, Pushkarev & Cawthorne 2000). If these two polarization orientations reflect different conditions in the core (e.g. more or less active), then it seems possible that the sources with aligned and misaligned radio-core and optical polarization could correspond predominantly to one orientation or the other ( $\chi_0 \parallel \Theta_j$  or  $\chi_0 \perp \Theta_j$ ). In order to estimate the direction of the jet, we searched for the position of some relatively representative features or components in the jet, which can be taken as good indicators of the jet direction. When possible, we searched for those features at our highest frequency,

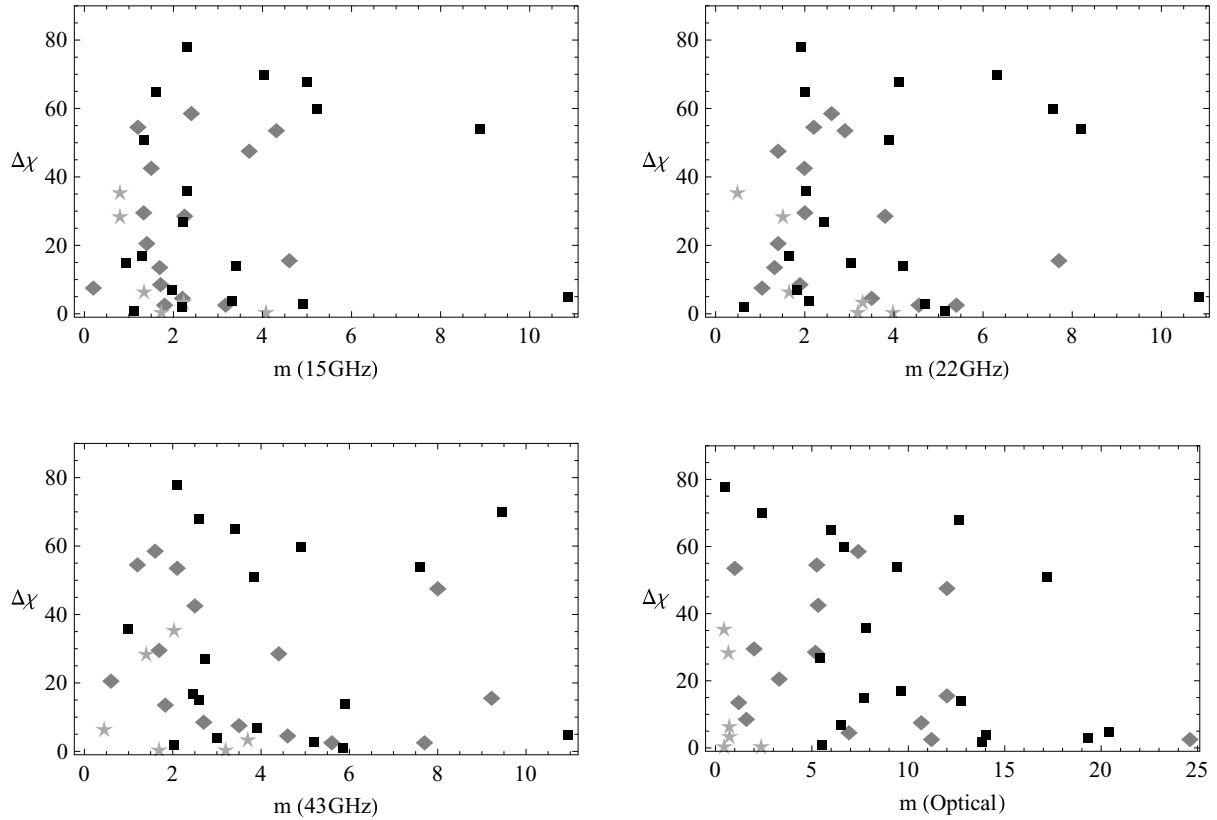


**Figure 8.** Comparison between  $\Delta\chi$  and the degree of polarization  $m$  obtained at 15, 22 and 43 GHz, and in the optical. BL Lacs are shown as black squares, HPQs are shown as grey diamonds and LPQs are shown as light grey stars.

43 GHz, so that we can avoid any features, such as jet bending or beam integration, that could mask the true direction of the base of the jet. We then calculated the direction of the jet, following the usual convention (i.e. origin in the north and increasing counter-clockwise). The estimation of the jet direction using this method is somewhat rough and we estimate that the associated uncertainty is typically around  $10^\circ$ .

We allowed the jet direction  $\Theta_j$  to run from  $-180^\circ$  to  $180^\circ$  and then we found the minimum difference between  $\chi_0$  values and  $\Theta_j$ . Results are given in Fig. 9. Angles have been set so that  $0^\circ \leq |\chi_0 - \Theta_j| \leq 90^\circ$ . It is clear that our data are widely scattered, and thus we find no evidence for a correlation between those two quantities;

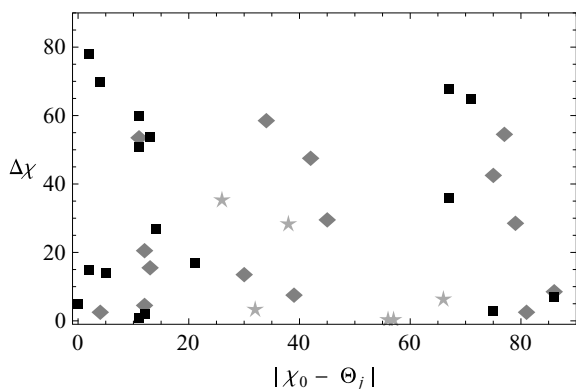


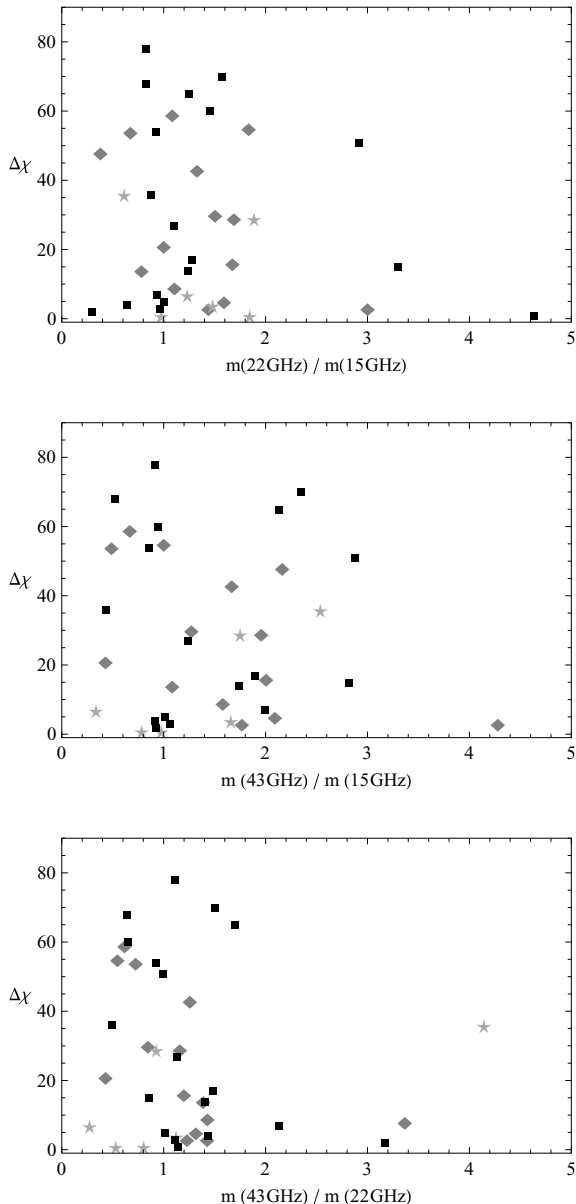
**Figure 9.**  $\Delta\chi$  plotted against the difference between the jet direction and the intrinsic radio-core polarization angle  $|\chi_0 - \Theta_j|$ . Symbols are the same as in Fig. 8.

in other words, there is no tendency for sources with small or large  $\Delta\chi$  to have  $\chi_0$  parallel or perpendicular to the jet direction.

### 4.3 The possibility of internal Faraday rotation

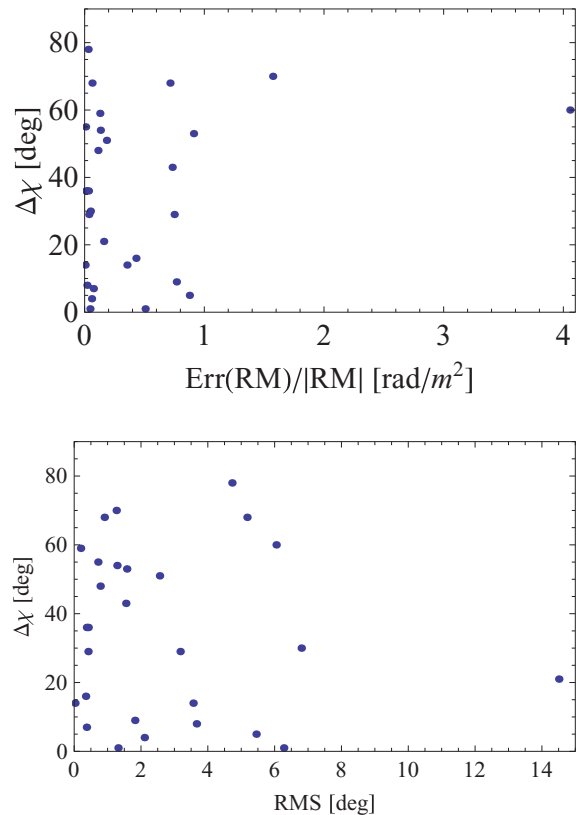
In the case of internal Faraday rotation, the rotation in  $\chi$  with  $\lambda^2$  is first linear and then saturates, with  $\Delta\chi$  further oscillating near values close to  $45^\circ$ – $50^\circ$  (Burn 1966). As discussed by Burn (1966), internal Faraday rotation also gives rise to a decrease of the core polarization at lower frequencies. To consider this fully, it would be necessary to analyse in detail the dependence of  $\chi$  and  $m$  on  $\lambda^2$ . Unfortunately, this is not possible with only three wavelengths. To investigate the possibility that the cores of some radio sources might be experiencing internal Faraday rotation, we used the depolarization factor, which we define here as the ratio of the degrees of core polarization at two different wavelengths. If the cores showing  $\Delta\chi \sim 50^\circ$  are those undergoing internal Faraday rotation, then they should also show high depolarizations. Indeed, depolarization due to internal Faraday rotation is expected to show a faster decline of the degree of polarization with  $\lambda$  than is expected for beam depolarization due to external Faraday rotation.

Fig. 10 shows a plot of  $\Delta\chi$  versus various depolarization factors. These plots suggest that a few of the cores could be experiencing appreciable depolarization, but this does not appear to be more true for the cores with  $\Delta\chi \sim 50^\circ$ . Most of the depolarization factors are fairly close to unity, indicating similar degrees of core polarization at all three radio frequencies. Only four sources have depolarization factors  $\frac{m(22\text{ GHz})}{m(15\text{ GHz})} > 2.5$ : 0745+241 ( $\Delta\chi = 51^\circ$ ), OJ287 at epoch GB ( $\Delta\chi = 3^\circ$ ), 0906+430 ( $\Delta\chi = 8^\circ$ ) and 1823+568 ( $\Delta\chi = 54^\circ$ ). In the same manner, only three sources have  $\frac{m(43\text{ GHz})}{m(22\text{ GHz})} > 2.5$ :



**Figure 10.** Depolarization factors for the sources in our sample. Symbols are the same as in Fig. 8.

2254+074 ( $\Delta\chi = 4^\circ$ ), 0906+430 ( $\Delta\chi = 8^\circ$ ) and 0953+470 ( $\Delta\chi = 36^\circ$ ). No sources with a significant higher depolarization factor are found for the group  $\frac{m(43\text{GHz})}{m(15\text{GHz})}$ . We note here that, with the exception of 0906+430, which appears in two of the cases, the rest of the sources having a high depolarization factor appear only once. Also, the  $\Delta\chi$  values found for those sources range over more than  $50^\circ$ , with no significant trend. Therefore, we conclude that there is no firm evidence that internal Faraday rotation is the cause of the misalignment between the optical and radio core position angles of a substantial number of sources in our sample. Another test that we performed was a check of the quality of the fits for the RM. In the presence of significant internal Faraday rotation, a  $\lambda^2$  law will no longer provide a good fit to the data and deviations from a linear RM fit should be appreciable. We can quantitatively measure this in two different ways: using the rms deviation for the fit and the relative error of the RM obtained. Both are shown in Fig. 11. For most of the sources, the rms deviations for their linear RM fits are



**Figure 11.** RM error (top panel) and rms deviation (bottom panel) of the observed values of  $\chi$  from the linear RM fit, plotted against  $\Delta\chi$ . The sources located farthest to the right-hand side in the upper and lower plots are 0256+075 and 0804+499, respectively.

less than about  $2^\circ$ , with only one source (0804+499) showing a very large rms  $\approx 14^\circ$ . There is no clear relation between rms and  $\Delta\chi$ . Similarly, the RM error appears to be independent of  $\Delta\chi$ .

We find no evidence that deviations from a  $\lambda^2$  law can provide an explanation for sources having  $\Delta\chi \sim 50^\circ$ . Therefore, there is no clear evidence for internal Faraday rotation that leads to deviations from a  $\lambda^2$  law and  $\Delta\chi$  values near  $50^\circ$ , although we cannot completely rule this out for all the sources.

#### 4.4 The possibility of high external Faraday rotation

As we observe at shorter wavelengths, we are probing smaller scales, where the electron density and magnetic field should increase, possibly giving rise to higher core Faraday rotation. For example, Jorstad et al. (2007) have presented evidence for 1–7 mm core RMs from several thousands to several tens of thousands of  $\text{rad m}^{-2}$ . In this case, there would be  $n\pi$  ambiguities in the measured polarization angles at our lower radio frequencies. However, the core RMs of quasars are typically higher than those for BL Lac objects (e.g. Zavala & Taylor 2004). Therefore, it is possible that such ambiguities did not arise in the previous work by Gabuzda et al. (2006), but affected the results presented here due to the high fraction of quasars in the overall sample.

Indeed, we have already found some evidence for relatively high core Faraday rotations in some of our sources. As was noted earlier, we applied modest rotations of  $\pi$  or  $2\pi$  rad to several of the observed angles at 22 and 15 GHz in order to obtain good  $\lambda^2$  fits (see Table 5). This indicates that at least some VLBI cores in our sample show

**Table 6.** Modified values of  $\chi$ , when high Faraday rotation is taken into account.

Source [1]	$\chi_{2\text{cm}}$ [2]	$\chi_{1.3\text{cm}}$ [3]	$\chi_{7\text{mm}}$ [4]	rms (high RM) [5]	rms (previous) [6]	$\chi_0$ [7]	$\Delta\chi$ [8]	RM (rad m <sup>-2</sup> ) [9]
0048–097	134 – 6 $\pi$	118 – 3 $\pi$	106 – $\pi$	0.8	0.4	50 ± 2	16	–45 200 ± 100
0133+476	–114 – 6 $\pi$	–116 – 3 $\pi$	–118 – $\pi$	1.1	0.2	–171 ± 2	6	–46 400 ± 150
0256+075	40 + 6 $\pi$	25 + 3 $\pi$	38 + $\pi$	4.8	6.0	84 ± 9	8	46 900 ± 650
0420–014	126 – 6 $\pi$	126 – 3 $\pi$	120 – $\pi$	0.3	1.5	69 ± 1	9	–46 400 ± 40
0745+241	73 + 5 $\pi$	88 + 2 $\pi$	108	1.4	2.6	–17 ± 3	77	44 900 ± 170
0745+241	73 – 6 $\pi$	88 – 3 $\pi$	108 – $\pi$	3.8	2.6	59 ± 7	1	–48 500 ± 480
1055+018	145 – 6 $\pi$	147 – 3 $\pi$	147 – $\pi$	0.9	0.3	96 ± 2	36	–46 800 ± 120
1510–089	53 – 6 $\pi$	58 – 3 $\pi$	55 – $\pi$	0.5	1.8	6 ± 1	44	–46 800 ± 50
1611+343	–32 – 6 $\pi$	–11 – 3 $\pi$	4 – $\pi$	2.1	0.4	–45 ± 4	25	–48 500 ± 320
1611+343	–32 + 6 $\pi$	–11 + 3 $\pi$	4 + $\pi$	1.2	0.4	62 ± 2	82	44 800 ± 200
1641+399	68 – 6 $\pi$	65 – 3 $\pi$	85 – $\pi$	6.6	5.5	31 ± 13	47	–47 400 ± 800
1641+399	68 + 6 $\pi$	65 + 3 $\pi$	85 + $\pi$	4.3	5.5	134 ± 8	56	45 900 ± 500
1652+398	171 + 6 $\pi$	–20 + 3 $\pi$	–166 + $\pi$	5.8	4.7	–160 ± 10	27	64 100 ± 600
1652+398	171 – 5 $\pi$	–20 – 2 $\pi$	–166	3.6	4.7	–83 ± 6	50	–29 300 ± 390
2251+158	–47 – 5 $\pi$	–65 – 2 $\pi$	–72	2.5	1.3	51 ± 5	2	–45 400 ± 340
OJ287	–41 – 6 $\pi$	–20 – 3 $\pi$	–3 – $\pi$	2.2	0.9	–52 ± 5	15	–48 500 ± 300
OJ287	–41 + 5 $\pi$	–20 + 2 $\pi$	–3	0.4	0.9	–126 ± 1	59	44 700 ± 60
3C279	–3 + 6 $\pi$	10 + 3 $\pi$	16 + $\pi$	2.2	0.8	73 ± 4	5	45 600 ± 300
3C279	–3 – 5 $\pi$	10 – 2 $\pi$	16	0.7	0.8	147 ± 1	79	–47 700 ± 100

evidence for relatively high Faraday rotation. This leaves us with another issue: have we identified all the sources in which this is happening? Are there other sources where we find a reasonable fit for the RM but, in fact, these do not correspond to the true RMs because high Faraday rotation is occurring in their cores?

To test this possibility, we obtained alternative fits for the RMs, allowing higher  $n\pi$  rotations in the polarization angles at 15 and 22 GHz. We assumed that  $\chi_{43\text{GHz}}$  is unaffected by this ambiguity due to its short wavelength or, at most, 180° can be added or subtracted to it, only to allow it to fall as near as possible to the optical value. Some number of  $\pi$  rad were then added or subtracted to the other values of  $\chi$  in order to obtain a good fit. A thin–thick transition (i.e. an extra addition of  $\pi/2$  rad in the angle corresponding to  $\chi_{15\text{GHz}}$ ) was allowed only when the core spectral index clearly showed this to be likely. For some sources, either no good alternate high RM fit was found or the fit obtained implied implausibly high RMs; we rejected the high-RM fits in these cases.

The results for acceptable high-RM fits are shown in Table 6. The first column shows the name of the source and the next three columns show the values of  $\chi$  utilized for each frequency (indicating the original  $\chi$  plus the number of rotations). The following columns show the rms of the high-RM fit and the previous rms from Table 5 for comparison. Finally, the following columns show the new  $\chi_0$ ,  $\Delta\chi$  and RM.

The results show that good  $\lambda^2$  fits can be obtained when these larger numbers of  $n\pi$  rotations are applied. The values of rms for many of the fits are small, comparable to the errors found in the values of  $\chi$  and essentially the same as in the original fits, or smaller in some cases. The core RMs obtained, though high, are of the order of tens of thousands of rad m<sup>-2</sup>, similar to those found by Jorstad et al. (2007), for example. As we noted above, high external Faraday rotation should produce significant beam depolarization, but the expected behaviour is not observed in either our own data or other VLBI-scale RM studies, such as that of Zavala & Taylor (2004); this may indicate that the observed ‘core’ includes contributions from a core region that is dominating the Faraday rotation and an inner jet region that is contributing significantly to the total observed degree of polarization. The absence of appreciable depolarization

may also indicate the action of an external Faraday screen that is nearly uniform.

Some of the new values of  $\Delta\chi$  are smaller than the original values, but this is not uniformly true. A number of sources admit several comparably good RM fits with different implied values of  $\Delta\chi$ . The high-RM fit for the HPQ 2251+158 shows  $\Delta\chi = 2$ , whilst, if our hypothesis were to be true, it should show  $\Delta\chi \sim 90$ , as it is optically thick at our radio frequencies (see Table 4).

Taken along with the original fits in Table 5, there may be several options for the RM that imply different intrinsic values of  $\chi_0$  and, therefore, different values of  $\Delta\chi$ . However, based on our current three-frequency VLBA data, *we cannot distinguish between these very different scenarios*.

Fig. 12 is an ‘optimistic’ version of the histogram in Fig. 6, in which we have tried to obtain the lowest possible values of  $\Delta\chi$  using the RMs in Table 6. Two important features can be noticed: (i) the peak near 50° has disappeared and (ii) a large fraction of the sources have their optical and VLBI-core EVPAs aligned within 20°. However, there is no justification for preferring the histogram in Fig. 12 over the one in Fig. 6. We are simply limited by our current

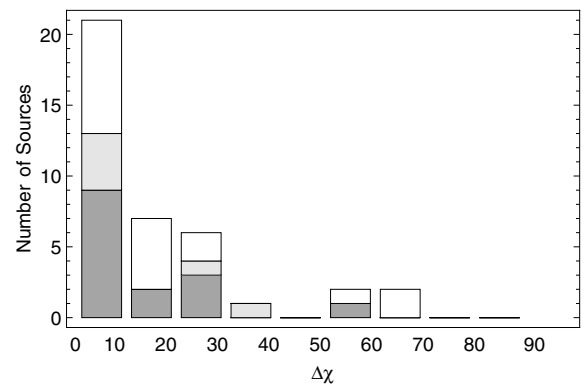


**Figure 12.** Same as Fig. 6, when high Faraday rotation is taken into account. Note that the peak near  $\sim 45^\circ$  is gone and most of the sources have now  $\Delta\chi < 30^\circ$ .



three-frequency data and cannot determine which distribution is closer to the real observational situation for these objects.

It would be interesting to try to test for the presence of high core RMs by comparing the observed values of  $\chi$  for the two neighbouring 15-GHz frequency bands making up the overall bandwidth at 15 GHz, which correspond to 15.277 49 and 15.285 49 GHz. However, the highest Faraday rotation suggested by our fits is  $\sim 64\,000$  rad m $^{-2}$ , which would give rise to a rotation of only  $\sim 1.5^\circ$  between these two frequencies – too small to detect, given our uncertainties in  $\chi$ .

## 5 CONCLUSIONS

In their earlier optical–VLBI polarization analysis for 11 BL Lac objects and the OVV quasar 3C279, Gabuzda et al. (2006) found nine out of 12 sources to have their optical and zero-wavelength VLBI core polarization angles aligned within  $20^\circ$ . Although less striking, we have likewise found evidence for a correlation between the simultaneously measured optical and 15–43 GHz VLBI core polarization angles, corrected for the Faraday rotation. The optical and VLBI core polarization angles are aligned to within  $20^\circ$  for 20 out of 37 objects (54 per cent), including the objects of Gabuzda et al. (2006). In five more objects,  $\chi_{\text{opt}}$  and  $\chi_0$  are aligned to within  $30^\circ$ . This behaviour can be understood if these are AGNs in which the optical and radio emission is essentially co-spatial. An appreciable number of the objects in our sample had differences between their optical and VLBI core polarization angles  $50^\circ < \Delta\chi < 70^\circ$ , apparently indicating that either their radio and optical emission is not co-spatial or the inferred values of  $\chi_0$  have been distorted by some process, such as internal or high external Faraday rotation.

The BL Lac objects and LPQs in the total sample of 37 AGNs show a tendency for their optical and VLBI-core polarization angles to be aligned. The HPQs show an almost flat distribution.

We emphasize here that there is no doubt that the  $\Delta\chi$  distribution in Fig. 6 is not random; this is true both for the distribution as a whole, and for the BL Lac objects and quasars on their own. We can test the hypothesis that the distribution is intrinsically random by assuming equal probability for  $\Delta\chi$  to be within each  $10^\circ$  bin, equal to 11.1 per cent, since there are nine bins. The probability for six of the BL Lac objects to be in the  $0^\circ \leq \Delta\chi \leq 10^\circ$  bin by chance is  $\sim 0.6$  per cent, according to a binomial probability distribution with a probability of 1/9 for a measurement to be in this bin and a probability of 8/9 for it to lie outside this bin. The probability for six or more BL Lac objects to be in this bin is  $\sim 0.8$  per cent. The corresponding probabilities for the LPQs are both  $\sim 0.2$  per cent, while they are  $\sim 1.5$  and  $\sim 2$  per cent for the HPQs. This shows that, although the values of HPQ  $\Delta\chi$  are only somewhat unlikely to come from a uniform distribution, the BL Lacs and LPQ  $\Delta\chi$  data are definitely inconsistent with a uniform distribution. In other words, the peak at  $\Delta\chi \sim 0^\circ$  is highly significant.

In a similar way, we can consider the statistical significance of the peak around  $\Delta\chi \sim 50^\circ$ . The probability for finding six (or six or more) sources in the  $50^\circ \leq \Delta\chi \leq 60^\circ$  bin by chance is both  $\sim 13$  per cent. Thus, although the visual appearance of the  $\Delta\chi$  distribution is suggestive of a secondary peak near  $50^\circ$ , this peak is currently only marginally significant.

The peak around  $\Delta\chi \sim 50^\circ$  may be due to the action of internal Faraday rotation in some quasar cores, although we have found no firm evidence for this. It also may be that we have mistakenly estimated some core RMs to be lower than their true values. If we allow for the possibility of high Faraday rotation, most of the sources could, in principle, show good alignments between their optical

and radio-VLBI core position angles. However, we are not able to distinguish between these cases with our current three-frequency data. This provided motivation to obtain new observations with additional radio frequencies, which could be used to more accurately determine the dependence of the values of radio  $\chi$  on  $\lambda^2$ , and thus deduce if the cores of particular sources are experiencing high external or internal Faraday rotation.

If  $\chi_{\text{opt}}$  and the associated intrinsic radio  $\chi_0$  are correlated, this implies that the emission regions at the two frequencies are co-spatial or at least that the magnetic field structure is the same over the range of scales on which the emission at the two frequencies is formed. This could even be on scales appreciably smaller than our current VLBI resolution. In this case, observations could be made for magnetic fields on scales unattainable directly using current VLBI techniques and directly comparable with theoretical models. If such correlations are ultimately shown to be common to essentially all AGNs, this will represent another important feature to be included in the AGN paradigm, taking us one step further in our understanding of the so-called Standard Model.

On the other hand, if only some AGNs or some types of AGNs show such a correlation, this also provides valuable information about the intrinsic physical differences between the different classes of AGNs (BL Lac objects, HQPs, LPQs). We have searched for some difference in the observational properties of the objects showing aligned and misaligned radio and optical polarization angles (degree of polarization, degree of depolarization, direction of  $\chi_0$  relative to the jet) that is correlated with  $\Delta\chi = |\chi_{\text{radio}} - \chi_{\text{opt}}|$  but without success so far. We will consider simultaneous optical and five-frequency 12–43 GHz VLBA polarization data designed to resolve  $\pi$  ambiguities in the values of radio  $\chi$  in our next paper.

## ACKNOWLEDGMENTS

This publication has emanated from research conducted with the financial support of Science Foundation Ireland. PSS acknowledges support from NASA/JPL/Spitzer contract 1256424. The National Radio Astronomy Observatory is operated by Associated Universities Inc. We thank the anonymous referee for helpful comments.

## REFERENCES

- Algaba J. C., 2010, PhD thesis, University College Cork
- Blumenthal G. R., Gould R. J., 1970, *Rev. Mod. Phys.*, 4, 237
- Burn B. J., 1966, *MNRAS*, 133, 67
- Croke S. M., Gabuzda D. C., 2008, *MNRAS*, 386, 619
- D’Arcangelo F. D. et al., 2007, *ApJ*, 659, L107
- Gabuzda D. C., 2003, *ApSS*, 288, 39
- Gabuzda D. C., Gómez J. L., 2001, *MNRAS*, 320, L49
- Gabuzda D. C., Sitko M. L., Smith P. S., 1996, *AJ*, 112, 1877
- Gabuzda D. C., Pushkarev A. B., Cawthorne T. V., 2000, *MNRAS*, 319, 1109
- Gabuzda D. C., Rastorgueva E. A., Smith P. A., O’Sullivan S. P., 2006, *MNRAS* 369, 1596
- Ghisellini G., Maraschi L., Treves A., 1985, *A&A*, 146, 204
- Jorstad S. G., Marscher A. P., Mattox J. R., Aller M. F., Aller H. D., Wehrle A. E., Bloom S. D., 2001, *ApJ*, 556, 738
- Jorstad S. G. et al., 2007, *AJ*, 134, 799
- Königl A., 1981, *ApJ*, 243, 700
- Kovalev Y. Y., Lobanov A. P., Pushkarev A. B., Zensus J. A., 2008, *A&A*, 483, 759
- Lister M. L., Smith P. S., 2000, *ApJ*, 541, 66
- Moore R. L., Stockman H. S., 1984, *ApJ*, 279, 465

Pacholczyk A. G., 1970, *Radio Astrophysics*, W. H. Freeman and Company, San Francisco  
Pohl M. et al., 1995, *A&A* 303, 383  
Reynolds C., Cawthorne T. V., Gabuzda D. C., 2001, *MNRAS*, 327, 1071  
Rudnick L., Owen F. N., Jones T. W., Puschell J. J., Stein W. A., 1978, *ApJ*, 225, L5  
Schmidt G. D., Stockman H. S., Smith P. S., 1992, *ApJ* 398, L57  
Smith P. S., Schmidt G. D., Hines D. C., Foltz C. B., 2003, *ApJ*, 593, 676

Smith P. S., Williams G. G., Schmidt G. D., Diamond-Stanic A. M., Means D. L., 2007, *ApJ*, 663, 118  
Stirling A. M. et al., 2003, *MNRAS* 341, 405  
Wardle J. F. C., Kronberg P. P., 1974, *ApJ*, 194, 249  
Zavala R. T., Taylor G. B., 2004, *ApJ*, 612, 749

This paper has been typeset from a  $\text{\TeX/L\AA\TeX}$  file prepared by the author.